Published in final edited form as:

Dev Cell. 2019 October 21; 51(2): 208–221.e6. doi:10.1016/j.devcel.2019.08.003.

An LRR Receptor-Teneurin System Directs Planar Polarity at Compartment Boundaries

Adam C. Paré[1,4,6], **Pooja Naik**[1,2,6], **Jay Shi**[1,3], **Zachary Mirman**[1,5], **Karl H. Palmquist**[1,5], **Jennifer A. Zallen**[1,7,*]

[1]Howard Hughes Medical Institute and Developmental Biology Program, Sloan Kettering Institute, New York, NY, USA

[2]Weill Cornell Graduate School of Medical Sciences, New York, NY, USA

[3]Weill Cornell/Rockefeller/Sloan Kettering Tri-Institutional MD-PhD Program, New York, NY, USA

[4]Present address: Department of Biological Sciences, University of Arkansas, AR, USA

[5]Present address: The Rockefeller University, New York, NY, USA

[6]These authors contributed equally

[7]Lead Contact

SUMMARY

Epithelial cells dynamically self-organize in response to extracellular spatial cues relayed by cell-surface receptors. During convergent extension in *Drosophila*, Toll-related receptors direct planar polarized cell rearrangements that elongate the head-to-tail axis. However, many cells establish polarity in the absence of Toll receptor activity, indicating the presence of additional spatial cues. Here we demonstrate that the leucine-rich-repeat receptor Tartan and the teneurin Ten-m provide critical polarity signals at epithelial compartment boundaries. The Tartan and Ten-m extracellular domains interact *in vitro*, and Tartan promotes Ten-m localization to compartment boundaries *in vivo*. We show that Tartan and Ten-m are necessary for the planar polarity and organization of compartment boundary cells. Moreover, ectopic stripes of Tartan and Ten-m are sufficient to induce myosin accumulation at stripe boundaries. These results demonstrate that the Tartan/Ten-m and Toll receptor systems together create a high-resolution network of spatial cues that guides cell behavior during convergent extension.

In Brief

*Correspondence: zallenj@mskcc.org.

AUTHOR CONTRIBUTIONS

A.C.P., P.N., and J.A.Z. conceived and designed the study. A.C.P., P.N., J.S., and K.H.P. did the experiments. Z.M. generated the new mutant alleles. A.C.P., P.N., J.S., K.H.P., and J.A.Z. analyzed the data. J.A.Z. supervised the study. A.C.P. and J.A.Z. wrote the paper with input from all authors.

SUPPLEMENTAL INFORMATION

Supplemental Information can be found online at https://doi.org/10.1016/j.devcel.2019.08.003.

DECLARATION OF INTERESTS

The authors declare no competing interests.

Compartment boundaries are conserved structures that prevent cell mixing in multicellular tissues. Paré et al. show that a system involving the LRR receptor Tartan and its teneurin ligand Ten-m position these boundaries by directing the subcellular localization of cytoskeletal regulators.

Graphical Abstract

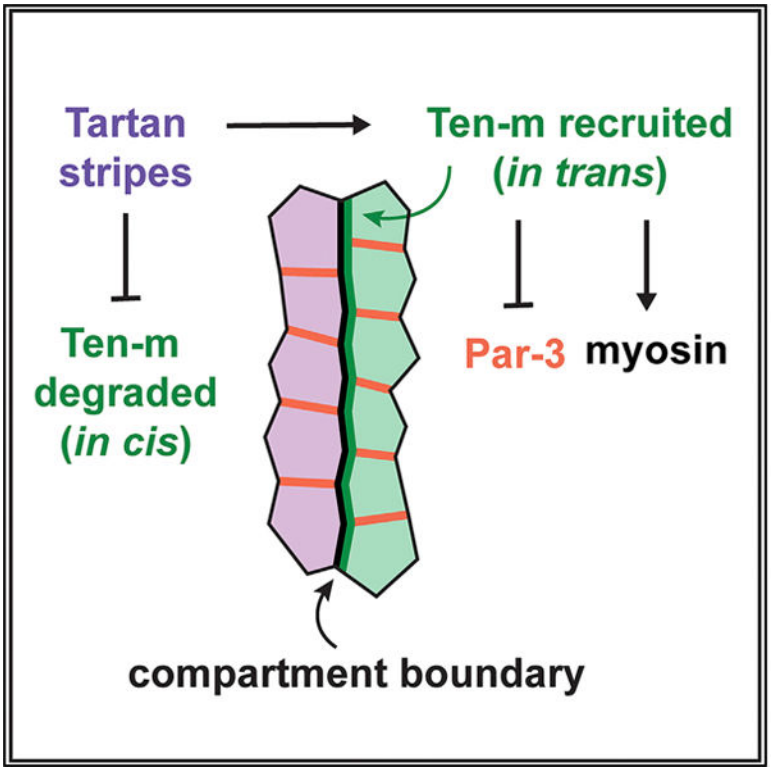

INTRODUCTION

Coordinated changes in cell shape and behavior transform epithelial sheets into elaborate grooves, tubes, branches, and compartments that are necessary for tissue and organ function. To carry out these choreographed structural changes, cells send, receive, and integrate spatial information from many sources. In the nervous system, myriad cell-surface interactions control axon guidance, target selection, and synapse formation to produce functional neural circuits (Zipursky and Sanes, 2010). A growing body of evidence suggests that a similarly rich repertoire of cell-surface proteins governs cell interactions in dynamically remodeling epithelia. Patterned gene expression underlies epithelial reorganization during development (Irvine and Wieschaus, 1994; Ninomiya et al., 2004; Zallen and Wieschaus, 2004; Paré et al., 2014), and local interactions between epithelial cells that express different receptors can induce cell polarization and sorting in mature tissues (Major and Irvine, 2005, 2006; Nishimura et al., 2007; Bielmeier et al., 2016). These findings suggest that the spatially regulated activity of cell-surface proteins is a fundamental strategy for epithelial self-organization. However, despite substantial progress in elucidating the cell-intrinsic mechanisms that control cell shape and behavior, it is not well understood how cell

behaviors are spatially coordinated across many cells to produce robust and reliable changes in tissue architecture.

A common mechanism for reshaping tissues is convergent extension, which elongates the head-to-tail body axis in developing embryos of worms, flies, chicks, frogs, and mice (Huebner and Wallingford, 2018). In *Drosophila*, elongation of the body axis requires precise patterns of gene expression and is a paradigm for understanding how planar polarized cell movements are organized at the tissue scale (Zallen and Blankenship, 2008; Lye and Sanson, 2011). In particular, striped patterns of pair-rule transcription factor activity confer distinct transcriptional identities to neighboring cells along the anterior-posterior (AP) axis, and these differences are required for the cell rearrangements that drive axis elongation (Irvine and Wieschaus, 1994; Zallen and Wieschaus, 2004). The cell-surface proteins that translate these gene expression patterns into oriented cell movements are only beginning to be identified. In the *Drosophila* embryo, robust cell intercalation requires three members of the conserved Toll receptor family, which are expressed in transverse stripes along the AP axis and provide positional cues that orient cell polarity and rearrangement (Paré et al., 2014). Best known for their roles in innate immunity and dorsal-ventral patterning (Morisato and Anderson, 1995; Brennan and Anderson, 2004), Toll receptors have also been shown to regulate cell and tissue morphogenesis (Kleve et al., 2006; Kolesnikov and Beckendorf, 2007; McIlroy et al., 2013; Carvalho et al., 2014; Meyer et al., 2014; Paré et al., 2014; Ward et al., 2015; Benton et al., 2016; Sun et al., 2017a). However, *Drosophila* embryos lacking striped Toll receptor expression still display substantial planar polarity (Paré et al., 2014), indicating that additional spatial cues remain to be discovered in this system.

Another important function of spatially regulated gene expression is to partition groups of cells within a continuous epithelium into functionally distinct compartments (Garcia-Bellido et al., 1973; Vincent and O'Farrell, 1992; Lawrence and Struhl, 1996; Monier et al., 2010). Epithelial compartments are often separated by actomyosin boundaries that prevent cell mixing between adjacent domains (Dahmann et al., 2011; Monier et al., 2011; Batlle and Wilkinson, 2012). However, the mechanisms that generate and position compartment boundaries are not well understood. In this study, we identify new roles for the leucine-rich repeat (LRR) receptor Tartan and the teneurin Ten-m in directing cell polarity and epithelial organization at compartment boundaries. We show that Tartan and Ten-m interact *in trans* in cultured cells, and that Tartan restricts Ten-m localization to compartment boundaries *in vivo*–where both proteins are required for planar polarity and boundary cell organization. This LRR receptor-Teneurin system controls cell polarity at epithelial compartment boundaries and acts together with patterned Toll receptor activity to create a high-resolution network of spatial cues that guides cell behavior and tissue organization in epithelia.

RESULTS

Toll-Independent Mechanisms Contribute to Planar Polarity at Compartment Boundaries

In the *Drosophila* embryo, convergent extension is driven by the planar polarized organization of proteins involved in actomyosin contractility and cell adhesion (Zallen

and Blankenship, 2008; Lye and Sanson, 2011). The nonmuscle myosin II motor protein and its upstream activators are concentrated at interfaces between neighboring cells along the AP axis (referred to as vertical edges), whereas Par-3 and adherens junction proteins are selectively depleted from these edges, resulting in spatially organized actomyosin contractility and cell intercalation (Bertet et al., 2004; Zallen and Wieschaus, 2004; Blankenship et al., 2006; Simões et al., 2010, 2014). Planar polarity is observed in the vast majority of cells in the germband epithelium (Zallen and Wieschaus, 2004; Tetley et al., 2016; Farrell et al., 2017), and requires the striped expression of three members of the Toll receptor family: Toll-2, Toll-6, and Toll-8 (Figures 1A and S1A–S1D) (Paré et al., 2014). However, it is not clear if Toll receptors control planar polarity throughout the entire tissue, or if additional spatial cues are required in specific regions to achieve robust planar polarity.

To distinguish between these possibilities, we analyzed myosin localization in Toll receptor-deficient embryos generated by injecting *Toll*-8 null mutants with dsRNAs targeting *Toll*-2 and *Toll*-6 (referred to as *Toll*-2,6,8 KD embryos). Myosin planar polarity was severely disrupted in *Toll*-2,6,8 KD embryos (Figures 1B and 1C), consistent with previous results in Toll receptor mutants (Paré et al., 2014). However, we noticed that myosin was still present in multicellular cables that repeated approximately every 4 cells (Figures 1B and 1C). The *Drosophila* germband consists of 14 compartments (parasegments), each of which contains 3–4 columns of cells, with even and odd compartments displaying distinct transcriptional profiles (Figures 1A and S1D) (Garcia-Bellido et al., 1973; Vincent and O'Farrell, 1992; Monier et al., 2010). The remaining myosin cables largely corresponded to the posterior borders of the Wingless stripes, which represent the posterior-most cells of each compartment (Figures 1A–1C). These results indicate that myosin planar polarity at compartment boundaries is correctly established in embryos deficient for Toll receptor activity.

To further characterize the spatial pattern of planar polarity in the absence of Toll receptor activity, we analyzed the distribution of Par-3 protein at single-cell resolution in *Toll*-2,6,8 triple mutant embryos. Par-3 is specifically depleted from vertical edges and enriched at horizontal edges in wild-type embryos, providing a strong readout of planar cell polarity (Zallen and Wieschaus, 2004; Simões et al., 2010). For these experiments, we generated new null mutations in all three receptor genes, including introducing a DsRed cassette flanked by attP sites into the *Toll*-2 and *Toll*-6 loci (Figure S2). As the embryonic epithelium consists of alternating even and odd compartments, we analyzed planar polarity at different positions within this repeating two-compartment unit (Figure S1D). Wild-type cells that contacted compartment boundaries (columns 1, 4, 5, and 8) displayed the strongest planar polarity, for both Par-3 (Figures 1D and 1E) and myosin (Tetley et al., 2016). In *Toll*-2,6,8 triple mutants, Par-3 planar polarity was reduced at multiple positions throughout the two-compartment unit. However, most cells that contacted compartment boundaries still displayed strong planar polarity (Figures 1D and 1E). To better characterize these defects, we measured the relative levels of Par-3 at different classes of cell edges (Figures 1E, 1G, and S1E). In *Toll*-2,6,8 mutants, the depletion of Par-3 from vertical edges was reduced at compartment boundaries (boundary edges) and at vertical edges within compartments (non-boundary edges) (Figures 1E–1G). However, boundary edges were still strongly polarized in the mutant embryos (2.6 ± 0.3-fold depletion of Par-3 from boundary edges in *Toll*-2,6,8 versus

3.1 ± 0.4-fold depletion in controls) (Figures 1E–1G). Par-3 levels at horizontal edges were comparable in control and mutant embryos (Figure S1F). Together, these results demonstrate that Toll receptors are required for planar polarity throughout the germband epithelium, but substantial planar polarity is still present at compartment boundaries in the absence of Toll receptor activity.

The LRR Receptor Tartan Directs Planar Polarity at Compartment Boundaries

To identify the spatial cues that control Toll-independent planar polarity at compartment boundaries, we investigated other cell-surface proteins that are expressed during convergent extension. Toll receptors belong to a large superfamily of proteins that contain extracellular leucine-rich repeats (LRRs), which includes 66 proteins in *Drosophila*, 135 proteins in mouse, 139 proteins in humans, and hundreds of proteins in plants, the majority of which are uncharacterized (Dolan et al., 2007; Ng et al., 2011; de Wit et al., 2011; Sun et al., 2017b). We hypothesized that the missing planar polarity signal at compartment boundaries could be an LRR receptor. In addition, it was predicted that a polarity cue expressed in alternating compartments is necessary for robust planar polarity in this tissue (Tetley et al., 2016). Based on these criteria, we decided to analyze Tartan–a transmembrane protein with 13 extracellular LRRs that is expressed in even compartments of the *Drosophila* embryo–as a candidate polarity signal (Chang et al., 1993). Tartan is required for epithelial cell sorting (Milán et al., 2001, 2005; Krause et al., 2006; Sakurai et al., 2007; Mao et al., 2008) and for axon and dendrite targeting in neurons (Kurusu et al., 2008; Hong et al., 2009), but the extracellular ligands and downstream effectors of Tartan are not known. We confirmed the striped expression of *tartan* using multiplex *in situ* hybridization and found that *tartan* is strongly expressed in columns 1–3 and weakly expressed in column 4 of even compartments (Figures 2A and 2B). To analyze Tartan function during convergent extension, we used CRISPR mutagenesis to generate a null allele that removes the entire *tartan* open reading frame and portions of the 5’ and 3’ UTRs (Figures S2D and S2G). In contrast to Toll-deficient embryos, *tartan* mutants displayed a selective loss of myosin cables at compartment boundaries, whereas myosin cables at non-boundary edges were maintained (Figures 2C and 2D). In addition, Par-3 depletion at compartment boundaries was significantly reduced in *tartan* mutants, with no change at non-boundary edges (Figures 2E–2G). These results demonstrate that Tartan is specifically required for planar polarity at compartment boundaries.

Tartan Interacts in *trans* with the Teneurin Ten-m

The extended array of LRRs in the Tartan extracellular domain suggests that Tartan interacts with extracellular proteins to carry out its functions. Despite numerous studies, no ligand for Tartan has been identified (Milán et al., 2001; Krause et al., 2006; Sakurai et al., 2007; Kurusu et al., 2008; Mao et al., 2008; Hong et al., 2009; Özkan et al., 2013). We used an *in vitro* assay for extracellular protein interactions (Özkan et al., 2013) to identify proteins that interact with Tartan. *Drosophila* S2R^{+} cells expressing candidate proteins were incubated with a soluble form of the Tartan extracellular domain (ECD) (Figure 3A). We found that the Tartan ECD selectively bound to cells expressing Ten-m (also known as *Tenascin-major* or *odz*), a member of the highly conserved teneurin protein family (Figures 3B and 3E). In the reciprocal experiment, the Ten-m ECD also bound to cells expressing full-length

Tartan (Figures 3B and 3F). Teneurins are dimeric type II transmembrane proteins with extracellular EGF-like, NHL (NCL-1, HT2A, and LIN-41), and YD (tyrosine and aspartic acid) repeats (Baumgartner et al., 1994; Levine et al., 1994; Oohashi et al., 1999) that are required for nervous system development in *Drosophila* (Hong et al., 2012; Mosca et al., 2012; Mosca, 2015; Baumgartner and Wides, 2019) and vertebrates (Leamey et al., 2007; Dharmaratne et al., 2012; Antinucci et al., 2013; Berns et al., 2018). Neither Tartan nor Ten-m displayed homotypic interactions (Figures 3B, 3E, and 3F) or heterotypic interactions with Toll receptors (Figures S3A–S3D) in this assay. These results demonstrate that the Tartan and Ten-m ECDs can interact *in vitro*, although it is unknown whether this interaction is direct or if it requires other cofactors present at the cell surface.

To investigate whether the Tartan/Ten-m interaction occurs *in cis* or *trans*, we mixed $S2R^+$ cells expressing Tartan–HA with untransfected cells and analyzed the localization of endogenous Ten-m protein using a monoclonal antibody to Ten-m (Levine et al., 1994) (see Figures S4E and S4F for antibody validation). Strikingly, Ten-m was strongly enriched at sites of contact between untransfected cells and Tartan-positive cells, but rarely accumulated at contacts between untransfected cells and cells expressing Toll receptors (Figure 3C). To determine whether Ten-m accumulates on the surface of Tartan-positive cells (*in cis*) or Tartan-negative cells (*in trans*), we used dsRNA to reduce Ten-m expression separately in each population (see Figure S4F for validation of *Ten-m* KD in $S2R^+$ cells). Reducing Ten-m expression in the Tartan-positive cell had no effect on Ten-m accumulation at sites of contact between Tartan-positive and Tartan-negative cells (Figures 3D and 3G). By contrast, reducing Ten-m expression in the Tartan-negative cell essentially eliminated Ten-m accumulation at cell-cell contacts. Furthermore, the addition of exogenous soluble Tartan ECD to the medium of untransfected cells induced the formation of Ten-m aggregates at the plasma membrane, which often colocalized with the soluble Tartan ECD (Figures S3E–S3G). These results demonstrate that Tartan and Ten-m can interact *in trans* in culture and that this interaction results in the accumulation of Ten-m at sites of cell-cell contact.

Ten-m Regulates Planar Polarity at Compartment Boundaries

These *in vitro* results reveal the teneurin Ten-m to be a previously unrecognized ligand for the LRR receptor Tartan. Teneurins are widely expressed in epithelia (Tucker et al., 2007), but few functions for this protein family have been identified outside of the nervous system (Drabikowski et al., 2005; Lossie et al., 2005; Kinel-Tahan et al., 2007; Zhang et al., 2018). *Ten-m* zygotic mutants were initially reported to have defects in embryonic patterning (Baumgartner et al., 1994; Levine et al., 1994), but this effect was later shown to be caused by an unrelated mutation (Zheng et al., 2011). Consequently, the effects of Ten-m on embryonic development are unknown. To characterize the role of Ten-m during convergent extension, we visualized Ten-m localization using the Ten-m antibody and a Ten-m– GFP fusion expressed from the endogenous locus (Lye et al., 2014). Ten-m protein was strongly enriched at the 8/1 compartment boundary and weakly enriched at the 4/5 compartment boundary (Figures 4A, 4B, and S4A). Ten-m protein at compartment boundaries was present throughout the apicolateral cell membrane (Figures S4A and S4B) and was detected both prior to and during convergent extension (stages 6–8, data not shown). Ten-m also localized to apical cell contacts in the vicinity of the adherens junctions in odd

compartments, but was largely absent from the membrane in even compartments, where it was instead present in cytoplasmic puncta (Figures 4A, 4B, and S4A). These results demonstrate that Ten-m subcellular localization is spatially patterned across the tissue, with a pronounced accumulation at compartment boundaries.

To ask if Ten-m has important functions at boundaries, we injected *Ten-m* dsRNA into early syncytial embryos prior to cellularization, in order to reduce maternal and zygotic Ten-m expression (referred to as *Ten-m KD* embryos). Although little maternal Ten-m protein was detected in wild-type embryo lysates from very young (0–2 h) embryos (Figure S4D), Ten-m protein was readily detectable at compartment boundaries in *Ten-m* zygotic mutants during convergent extension (~3–4 h, data not shown), indicating that Ten-m protein at this stage is generated, at least in part, from maternally supplied transcripts. *Ten-m* dsRNA injection reduced Ten-m protein levels during convergent extension by ~90% (Figure S4E) and resulted in a complete loss of Ten-m protein from compartment boundaries (data not shown). Par-3 edge polarity was significantly disrupted at compartment boundaries in *Ten-m* KD embryos, with no defects in Par-3 localization at non-boundary edges (Figures 4E–4G), similar to *tartan* mutants. In addition, *Ten-m* KD resulted in a significant reduction of myosin cables at compartment boundaries compared with water-injected controls (Figures 4C and 4D). Comparable defects were observed in embryos injected with a second dsRNA targeting a different exon of *Ten-m* (Figure S5). *Ten-m* KD embryos also displayed subtle defects in myosin localization at non-boundary edges (Figures 4D and S5D), which we also observed in embryos injected with *tartan* dsRNA (not shown), but not in *tartan* null mutants (Figures 2C and 2D), suggesting that myosin localization at non-boundary edges may be susceptible to nonspecific mechanical perturbations caused by embryo injection. Together, these results demonstrate that Tartan and Ten-m are required for planar polarity at compartment boundaries.

Tartan Restricts Ten-m Localization to Compartment Boundaries

As *Ten-m* is predicted to be an extremely large gene (>100 kb), there is unlikely to be sufficient time to transcribe zygotic *Ten-m* mRNA in a striped pattern during convergent extension. Therefore, we speculated that Ten-m could be regulated by Tartan post-transcriptionally. Consistent with this hypothesis, simultaneous detection of both proteins using available antibodies (Chang et al., 1993; Levine et al., 1994) revealed that Ten-m cables correlated with the edges of Tartan stripes (Figure 5A). Ten-m protein accumulated strongly at the anterior boundary and more weakly at the posterior boundary of each Tartan stripe, and Tartan and Ten-m frequently colocalized at compartment boundaries and in cytoplasmic puncta in even compartments (Figures 5A and 5B). To test whether Tartan is required for Ten-m localization, we analyzed Ten-m localization in *tartan* mutants. Ten-m was no longer recruited to compartment boundaries in *tartan* mutants, and instead localized to all cell contacts, reminiscent of odd compartment cells in wild type (Figures 5C, 5D, 5G, and 5H). These results suggest that all germband cells have the capacity to produce Ten-m protein, but Ten-m membrane localization is inhibited in even compartments and enhanced at compartment boundaries in response to striped Tartan expression.

To further examine the effect of Tartan on Ten-m localization, we misexpressed Tartan throughout the embryo using a maternal Gal4 driver. Ubiquitous Tartan expression resulted in a complete loss of Ten-m from the plasma membrane, and Ten-m was instead distributed in cytoplasmic puncta in all cells (Figures 5E, 5G, and 5H). Ten-m protein levels were reduced by approximately half in Tartan-overexpressing embryos, indicating that Tartan negatively regulates Ten-m levels (Figure S4C). By contrast, Ten-m localization occurred normally in embryos defective for Toll receptor activity (Figures 5F and 5G). These *in vitro* and *in vivo* results suggest that Tartan shapes the distribution of Ten-m in two ways: by downregulating Ten-m membrane localization *in cis* in even compartments, and by promoting Ten-m accumulation at compartment boundaries, potentially through *trans* interactions at Tartan stripe borders.

Local Differences in Tartan and Ten-m Induce Cell Polarity and Alignment

A critical function of compartment boundaries is to create barriers that inhibit cell mixing between compartments. This boundary function requires a local increase in actomyosin contractility (Major and Irvine, 2005, 2006; Landsberg et al., 2009; Monier et al., 2010; Tetley et al., 2016). A hallmark of planar polarized myosin activity is the alignment of multiple consecutive cell contacts to create straight borders between adjacent tissue domains (Landsberg et al., 2009; Monier et al., 2010). To determine whether Tartan and Ten-m are required for this property of boundary cells, we measured the degree of cell alignment by calculating the ratio of the measured boundary length to the theoretical shortest path (the length ratio) (Figures 6A and 6B). In *tartan* mutant and *Ten-m* KD embryos, the compartment boundary length ratio was significantly increased, indicating a defect in actomyosin contractility at boundaries (Figure 6B, top). By contrast, the non-boundary length ratio at the column 7/8 boundary was unaffected (Figure 6B, bottom). These results demonstrate that Tartan and Ten-m are necessary for proper boundary cell morphology.

If compartment boundaries are generated in response to sharp differences in receptor levels or activity, then eliminating these differences should prevent Tartan and Ten-m from acting as polarity cues. To investigate this possibility, we expressed Tartan or Ten-m ubiquitously throughout the embryo to swamp out their endogenous expression patterns. Indeed, uniform expression of Tartan or Ten-m disrupted cell alignment at compartment boundaries, similar to the defects caused by loss of either protein (Figure 6B). We next asked whether sharp differences in Tartan or Ten-m expression are sufficient to induce ectopic myosin accumulation. To test this, we used the engrailed-Gal4 driver to ectopically express Tartan and Ten-m in stripes in the late embryonic epidermis, a tissue that does not normally show strong myosin polarity. Ectopic stripes of Ten-m or Tartan both induced strong myosin accumulation at the anterior border of the engrailed expression domain, reminiscent of myosin cables at compartment boundaries (Figures 6C and 6D). Together, these results demonstrate that local differences in Tartan and Ten-m activity are necessary for myosin planar polarity and boundary morphology and are sufficient to induce myosin planar polarity in other tissues.

Tartan and Toll Receptors Act in Parallel during Convergent Extension

If the Tartan/Ten-m and Toll receptor systems are the two major mechanisms that generate planar polarity during convergent extension—Toll receptors acting within compartments and Tartan/Ten-m receptors acting at compartment boundaries— then removing both systems should disrupt planar polarity throughout the tissue. To test this, we generated quadruple-mutant embryos that completely lack zygotic *tartan*, *Toll-2*, *Toll-6*, and *Toll-8* expression using CRISPR engineering (Figure S2) (Port et al., 2015). Quadruple-mutant embryos lack patterned spatial cues from both the Toll receptor and Tartan/Ten-m systems, as the loss of *tartan* disrupts patterned Ten-m localization (Figures 5D and 5G). Indeed, embryos lacking all four LRR receptors displayed a profound loss of Par-3 planar polarity in all cell columns (Figures 7A–7C and S6A). Residual Par-3 planar polarity was still detected in the vicinity of column 5 in quadruple-mutant embryos (Figure 7A), suggesting that additional signals contribute to planar polarity in this region. These results demonstrate that Tartan and the Toll receptors act in parallel in distinct regions of the tissue to generate robust planar polarity during convergent extension.

To determine how the loss of both Tartan/Ten-m and Toll receptor systems affects cell behavior, we analyzed cell intercalation in time-lapse movies of embryos during convergent extension (Figures 7D–7F; Video S1). Whereas 1.92 ± 0.05 edges contracted/cell in wild-type embryos, the loss of *tartan* alone led to a slight increase in cell intercalation (2.21 ± 0.06 edges contracted/cell in *tartan* mutants, mean ± SEM, $p < 0.02$) (Figure 7E). By contrast, cell intercalation was severely disrupted in quadruple mutants lacking all four LRR receptors (Figure 7D). The number of intercalation events was reduced by nearly half in quadruple mutants compared with wild type (1.08 ± 0.10 edges contracted/cell, $p < 0.0001$ versus wild type), and was significantly more defective than in *Toll-2,6,8* triple mutants (1.40 ± 0.08 edges contracted/cell, $p < 0.0001$ versus wild type and $p < 0.01$ versus the quadruple mutant) (Figure 7E). We speculate that some classes of cell rearrangement may normally be inhibited at compartment boundaries and the loss of *tartan* could lead to increased cell movement in these regions. By contrast, the loss of *tartan* in Toll-defective embryos that already have compromised myosin activity could lead to decreased intercalary behavior throughout the tissue—potentially explaining why *tartan* exacerbates the defects in *Toll-2,6,8* mutant embryos (Figures 7E and 7F). As a result of the overall loss of spatial information in quadruple-mutant embryos, errors occurred at some step of intercalation in 54 ± 3% of intercalation attempts, a more than 2.5-fold increase over wild-type levels (21 ± 3%) ($p < 0.0001$) (Figure S6B). In addition, axis elongation was reduced by nearly half in embryos lacking all four LRR receptors, compared with approximately one-third for *Toll-2,6,8* triple mutants (Figure 7F). Together, these results demonstrate that the Tartan/Ten-m and Toll receptor systems act in parallel to regulate planar polarity and cell behavior during convergent extension.

DISCUSSION

Diverse ligand and receptor molecules promote selective cell interactions to mediate cell-pathogen and axon-target recognition in the immune and nervous systems. Our results provide evidence that a similar diversity is present in epithelial tissues, in which two distinct

polarity systems act in parallel to encode spatial information during epithelial remodeling in the *Drosophila* embryo. In particular, we show that the LRR receptor Tartan and the teneurin Ten-m work together to direct planar polarity and actomyosin contractility at compartment boundaries during convergent extension. These results demonstrate an essential role for teneurins in epithelial organization and show that Tartan is necessary for compartment boundary formation in the elongating germband, extending previous findings that Tartan is sufficient to induce boundary formation in the *Drosophila* wing (Milán et al., 2001; Mao et al., 2008). We provide evidence for a molecular connection between the LRR and teneurin protein families–identifying the first known ligand for Tartan and expanding the range of ligands for teneurins beyond their previously described binding partners (Rubin et al., 2002; Hong et al., 2009; Silva et al., 2011; Boucard et al., 2014; Mosca, 2015; Berns et al., 2018). Tartan restricts Ten-m localization to compartment boundaries *in vivo*, and local differences in Tartan and Ten-m activity are necessary and sufficient for planar polarity and compartment boundary structure. Together, the Tartan/Ten-m and Toll receptor systems act in parallel to generate dense, high-resolution networks of spatial cues that direct cell polarity and behavior during epithelial remodeling.

Patterned receptors provide critical spatial inputs that promote planar polarity in epithelial tissues, indicating that cells are exquisitely sensitive to local differences in the level or activity of cell-surface proteins (Irvine and Wieschaus, 1994; Zallen and Wieschaus, 2004; Zallen, 2007; Paré et al., 2014). Teneurins are expressed in complex patterns in the nervous system and participate in homotypic and heterotypic interactions that control proper neural connectivity (Rubin et al., 2002; Hong et al., 2009; Mosca, 2015; Berns et al., 2018). However, we believe that the spatial pattern of Ten-m during convergent extension is unlikely to result from patterned transcriptional regulation, for several reasons. These include the large size of the *Ten-m* gene (>100 kb), the short time between the onset of zygotic gene expression and patterned Ten-m localization, and the distinct subcellular distributions of Ten-m protein in even and odd compartments. Instead, we favor a model in which Tartan regulates Ten-m localization post-transcriptionally. Our *in vitro* and *in vivo* results suggest that Tartan influences the distribution of Ten-m in two ways. First, Tartan inhibits Ten-m localization to the membrane *in cis* in even compartments. In support of this model, Ten-m protein normally only localizes to the membrane of cells in odd compartments that lack Tartan, and Ten-m localizes to the membrane of all cells in *tartan* mutants. These results suggest that Tartan inhibits Ten-m membrane localization when these proteins are expressed in the same cell, perhaps by altering Ten-m trafficking, destabilizing the Ten-m protein, or competing for factors required for Ten-m membrane localization. Second, our *in vitro* results indicate that Tartan can stabilize Ten-m localization at the membrane of neighboring cells, raising the possibility that *trans* interactions between these proteins recruit Ten-m to the borders of Tartan stripes *in vivo*, establishing compartment boundaries. Tartan and Ten-m are both required for the localized recruitment of myosin and exclusion of Par-3, two proteins that are important for boundary structure (Landsberg et al., 2009; Monier et al., 2010; Urbano et al., 2018). It remains to be determined whether Tartan or Ten-m is the ligand or receptor in this interaction, or if their interaction triggers bidirectional signaling downstream of both receptors. This dual mechanism of Ten-m regulation by Tartan is reminiscent of Notch signaling, in which the Notch receptor is activated by

ligands expressed in neighboring cells, but inhibited by ligands expressed in the same cell (del Álamo et al., 2011), and the core Frizzled/Van Gogh planar cell polarity (PCP) pathway, in which *trans*-acting positive interactions and *cis*-acting inhibitory interactions sort proteins into distinct membrane domains (Peng and Axelrod, 2012; Yang and Mlodzik, 2015). Combined *cis*-inhibition and *trans*-activation may be a general strategy for mobilizing ubiquitously expressed proteins in spatially restricted patterns to provide localized positional cues.

A growing number of receptors have been shown to induce localized myosin activity at sites where receptor levels or activity differ between neighboring cells (Major and Irvine, 2005, 2006; Nishimura et al., 2007; Bielmeier et al., 2016). Our findings demonstrate that molecularly distinct receptors–Toll receptors, the LRR receptor Tartan, and the teneurin Ten-m–all contribute to planar polarized myosin activity during convergent extension (Paré et al., 2014 and this study). The mechanisms by which these diverse receptor families communicate to the actomyosin contractile machinery are not known. As the Tartan/Capricious, Teneurin, and Toll receptor families have unrelated intracellular domains, an intriguing possibility is that the receptors acting at compartment boundaries could have distinct cell biological outputs. Cells that border compartment boundaries display unique behaviors that prohibit crossing into neighboring domains (Landsberg et al., 2009; Monier et al., 2010; Umetsu et al., 2014; Scarpa et al., 2018). Tartan and Ten-m may impart distinct molecular properties to boundary cells which, together with Wingless signaling (Vincent and O'Farrell, 1992; Larsen et al., 2008), could prime them to serve as long-term barriers to cell movement. Actomyosin networks are present at compartment boundaries in *Xenopus* (Fagotto et al., 2013), zebrafish (Calzolari et al., 2014), and mice (Galea et al., 2017), and are critical for the establishment and maintenance of tissue structure. Given the widespread expression of teneurins and members of the extremely diverse LRR receptor family in epithelia, the spatially localized activities of these receptors could be a general mechanism for regulating multicellular organization during epithelial morphogenesis.

STAR★METHODS

LEAD CONTACT AND MATERIALS AVAILABILITY

Fly lines and plasmids generated in this study are available upon request. Further information and requests for resources and reagents should be directed to and will be fulfilled by the Lead Contact, Jennifer Zallen (zallenj@mskcc.org).

EXPERIMENTAL MODEL AND SUBJECT DETAILS

***Drosophila* Stocks and Genetics—**Wild-type embryos were Oregon R and control genotypes are indicated for each experiment. *Drosophila* adults were reared on molasses/cornmeal/yeast food and embryos were collected on apple juice agar plates at 25°C. Embryo stages are indicated in the figure legends. The sex of the embryos was not considered relevant to this study and was not determined. Mutant chromosomes generated by CRISPR-mediated genome engineering in this study were: *Toll-2*^{attP} (*Toll-2* ORF replaced with attP-3XP3-DsRed-attP); *Toll-6*^{attP} (*Toll-6* ORF replaced with attP-3xP3-DsRed-attP); *Toll-8*$^{\Delta 6B}$, *Toll-6*^{attP} (deletion of *Toll-8* ORF on the *Toll-6*^{attP} chromosome);

tartan^{3C} (deletion of *tartan* ORF); *tartan*^{3A}, *Toll-8*$^{\Delta 6B}$, *Toll-6*^{attP} (deletion of *tartan* ORF on the *Toll-8*$^{\Delta 6B}$, *Toll-6*^{attP} chromosome). The following recombinant chromosomes were generated in this study: myosin–GFP, *Toll-8*^{59}; *Toll-8*$^{\Delta 6B}$, *Toll-6*^{attP}, *spider–GFP*; *tartan*^{3C}, *spider–GFP*; and *tartan*^{3A}, *Toll-8*$^{\Delta 6B}$, *Toll-6*^{attP}, *spider–GFP*. New transgenes were *UASp-tartan–HA* (VK37) and *UASp-HA-Ten-m* (attP2). Other stocks and alleles were *Toll-2*$^{\Delta 76}$ (used in Figure 5G only) (deletion of 450 bp in the *Toll-2* ORF and 2.3 kb upstream sequence) (Kleve et al., 2006), *Toll-8*^{59}, *Toll-6*^{1B} (used in Figure 5G only) (early frameshift mutation in *Toll-6* and a deletion of the entire *Toll-8* open reading frame) (Paré et al., 2014), *Toll-8*^{59} (Yagi et al., 2010) and *Toll-8*^{145} (Kolesnikov and Beckendorf, 2007) (used in Figures 1B and 1C), the *Ten-m*$^{CPTI\ -001175}$ endogenous GFP tag (Lye et al., 2014), *Spider–GFP* and *Resille–GFP* (gifts of Alain Debec), *myosin–GFP* (GFP fused to the myosin regulatory light chain *sqh* expressed from the *sqh* promoter) (Royou et al., 2004), and *engrailed-Gal4* recombined with *UASp-mCherry–Moesin* (mCherry fused to the F-actin-binding domain of Moesin) (Millard and Martin, 2008).

To genotype mutant embryos for Par-3 polarity analysis in *Toll-2,6,8* triple mutants, *tartan* single mutants, and *tartan, Toll-2,6,8* quadruple mutants, males and females heterozygous for the desired mutations (without balancers) were crossed together, and homozygous mutant embryos were identified by *in situ* hybridization based on lack of appropriate mRNA signal. For myosin analysis in *tartan* mutants, homozygous mutant embryos were identified by the absence of staining with a guinea-pig anti-Tartan antibody. The mutant genotypes and the corresponding controls in Figures 6A and 6B were: *tartan* (*myosin–GFP*/+; *trn*^{3C}), control for *tartan* (*myosin–GFP*/+; *trn*^{3C}/+ or +/+), *Ten-m* KD (*myosin–GFP* injected with *Ten-m* dsRNA), control for *Ten-m* KD (*myosin–GFP* injected with water), Tartan OE (progeny of females heterozygous for maternal α-tubulin67 and maternal α-tubulin15 Gal4 drivers and *UASp-Tartan-HA*), Ten-m OE (progeny of females heterozygous for maternal α-tubulin67 and maternal α-tubulin15 Gal4 drivers and *UASp-HA-Ten-m*), controls for Tartan OE and Ten-m OE (progeny of females heterozygous for maternal α-tubulin67 and maternal α-tubulin15 Gal4 drivers processed in parallel). The genotypes in Figures 6C and 6D were: control (*en-Gal4, UASp-mCherry–Moesin/+; myosin–GFP*/+), en>Tartan (*en-Gal4, UASp-mCherry–Moesin/UASp-tartan–HA; myosin– GFP*/+), en>Ten-m (*en-Gal4, UASp-mCherry–Moesin/+; myosin–GFP/UASp-HA–Ten-m*).

To genotype mutant embryos in live-imaging experiments, males and females heterozygous for the desired mutations over a *CyO*, *twist-Gal4*, *UAS-GFP* balancer (II) and/or an *eve–YFP* BAC insertion (in attP2 on III) (Ludwig et al., 2011) were crossed, and embryos homozygous for second- and third-chromosome mutations were selected based on the absence of GFP and/or YFP expression.

Cell Culture Conditions—S2R^{+} cells were maintained at 25°C in Schneider's medium supplemented with 10% fetal calf serum (Sigma).

METHOD DETAILS

Fluorescence In Situ Hybridization and Immunofluorescence in Embryos—Primary antibodies for immunohistochemistry were guinea pig anti-Par-3 (1:250 for

simultaneous mRNA/protein detection and 1:500 for immunofluorescence) (Blankenship et al., 2006), mouse anti-Ten-m (mAb20 generated to a region overlapping the last 4 EGF-like repeats, 1:300–1:500) (Levine et al., 1994), mouse anti-wingless (1:25–1:50; Developmental Studies Hybridoma Bank, 4D4) (Brook and Cohen, 1996), rabbit anti-GFP (1:125–1:150, Torrey Pines), rabbit anti-Tartan (1:400) (Chang et al., 1993) (used in Figures 5A and 5B), and guinea pig anti-Tartan (1:100) (Mao et al., 2008) (used to genotype *tartan* mutant embryos in Figures 2C and 2D). The *UASp-mCherry–Moesin* marker (Millard and Martin, 2008) was used to label engrailed-Gal4-expressing cells and was visualized with a mouse Living Colors mCherry antibody (1:50; Takara). Primary antibodies were detected with Alexa Fluor-labeled secondary antibodies (1:500; Molecular Probes). Embryos were mounted in ProLong Gold (Molecular Probes) and imaged on a Zeiss LSM700 laser-scanning confocal microscope with a PlanNeofluor 40×1.3 NA oil-immersion objective; z-slices (1.0-μm thick) were acquired in steps of 0.45–0.5 μm.

To analyze Par-3 localization in *Toll-2,6,8* triple-mutant, *tartan* single-mutant, and *tartan,Toll-2,6,8* quadruple-mutant embryos, simultaneous mRNA/protein detection was performed using the acetone permeabilization method, as previously described (Paré et al., 2009). Embryos were fixed for 25 min a 1:1 solution of heptane:9% formaldehyde (Sigma) and 50 mM EGTA in PBS and devitellinized in a 1:1 solution of heptane:methanol. To detect *Toll-2, Toll-6*, and *Toll-8*, antisense RNA probes were transcribed with T7 polymerase from *pEntr-Toll-2*, *pEntr-Toll-6*, and *pEntr-Toll-8* plasmids containing the full-length open reading frames (Paré et al., 2014) linearized with NotI. To detect *tartan*, antisense RNA probes were transcribed with SP6 polymerase from the GH10871 plasmid (*Drosophila* Genomics Resouce Center) containing the *tartan* cDNA linearized with EcoRV. To detect *wg*, antisense RNA probes were transcribed from a PCR-amplified template and transcribed with T7. See Table S1 for primer sequences. Probes were labeled with digoxigenin-UTP or dinitrophenyl-UTP, and bound probes were detected with mouse anti-digoxigenin (1:250; Jackson ImmunoResearch) or rabbit anti-dinitrophenyl (1:250; Molecular Probes) antibodies. To analyze Par-3 localization in *Ten-m* KD embryos, *Ten-m–GFP* embryos were injected with water (control) or 2 μg/μl *Ten-m* KD dsRNA, fixed for 25 min in a 1:1 solution of heptane and 9% formaldehyde (Sigma) in PBS, manually devitellinized, and stained in the same tube. *Ten-m* KD embryos were selected by the absence of Ten-m–GFP signal. To analyze Par-3 localization in *Ten-m* KD2 embryos, Oregon-R (wild-type) embryos were injected with water (control) or 2 μg/μl *Ten-m* KD2 dsRNA, fixed for 25 min in a 1:1 solution of heptane and 9% formaldehyde (Sigma) in PBS, manually devitellinized, and stained in the same tube after prestaining the control embryos with Alexa 488-conjugated phalloidin (1:1,000; Molecular Probes). For Par-3 cell and edge polarity analyses, embryos were compared to internal controls (including heterozygotes) processed in the same tube to minimize experimental variability. Each result is representative of at least two independent experiments.

To analyze myosin localization in *Toll-2,6,8* KD embryos, the progeny of *myosin–GFP, Toll-8*^{59}*/Toll-8*^{145} males and females were injected with dsRNAs targeting *Toll-2* and *Toll-6* (1 μg/μl each); control embryos were the heterozygous progeny of *Toll-8*^{59}, *myosin–GFP*/+ males and females injected with water. To analyze myosin localization in *Ten-m* KD and *Ten-m* KD2 embryos, *myosin–GFP* embryos were injected with 2 μg/μl *Ten-m* KD dsRNA,

Ten-m KD2 dsRNA, or water (control). Embryos were fixed in a 1:1 solution of heptane and 37% formaldehyde (Sigma) for 5 min and then manually devitellinized (Figures 1B, 1C, 2C, 2D, 4C, 4D, 6A and the loss of function conditions in 6B). For the analysis of boundary and non-boundary length ratios in the overexpression conditions in Figure 6B, embryos were fixed 30 min in a 1:1 solution of heptane and 4% paraformaldehyde (Electron Microscopy Sciences) in PBS and devitellinized in 1:1 heptane:methanol. For the analysis of myosin–GFP localization in stage 15 embryos, embryos were fixed 30 min in a 1:1 solution of heptane and 3.7% formaldehyde (Sigma) in PBS and devitellinized in 1:1 heptane:methanol.

To analyze Ten-m localization in wild-type, *tartan* mutant, and Tartan-overexpressing embryos, embryos were fixed for 30 min in a 1:1 solution of heptane and 4% paraformaldehyde (Electron Microscopy Sciences) in PBS and devitellinized in 1:1 heptane:methanol. To analyze Ten-m localization in *Toll-2,6,8* mutants and internal controls, embryos were fixed using the acetone permeabilization method (Paré et al., 2009). To visualize Ten-m–GFP, embryos were fixed for 25 min in a 1:1 solution of 9% formaldehyde (Sigma) in PBS and manually devitellinized. Staining for endogenous Ten-m using the Ten-m antibody and the 4% paraformaldehyde fixation protocol, or staining for Ten-m–GFP using the GFP antibody and 9% formaldehyde fixation protocol, revealed all three characteristics of Ten-m localization depicted in Figure 4B: Ten-m cables at compartment boundaries starting at the adherens junctions and continuing sporadically throughout the lateral membrane, apical Ten-m membrane localization in odd compartments, and basolateral Ten-m puncta in even compartments. By contrast, staining for endogenous Ten-m using the acetone permeabilization method detected Ten-m cables at compartment boundaries, but only in more apical regions (within a few microns of the apical surface). In addition, this method detected apical Ten-m membrane localization in odd compartments, but did not detect strong Ten-m signal at compartment boundaries in more basolateral positions or the basolateral Ten-m puncta in even compartments.

dsRNA Injection—For RNA interference, dsRNAs were designed using the E-RNA*i* website (Horn and Boutros, 2010) to minimize off-target effects. *Toll-2* and *Toll-6* dsRNAs were generated as described (Paré et al., 2014). *Ten-m* KD and *Ten-m* KD2 embryos were injected with dsRNAs targeting nonoverlapping regions of the *Ten-m* gene. DNA templates containing T7 promoters at their 5’ and 3’ ends were generated using the odz_dsRNA_f and odz_dsRNA_r primers (for *Ten-m* KD, targeting the last exon) or the Ten-m_KD2_f and Ten-m_KD2_r primers (for *Ten-m* KD2, targeting the second-to-last exon). The dsRNAs were transcribed using the T7 MEGAscript Kit (Ambion) and diluted in H_2O as described (Paré et al., 2014). Embryos were collected for 1 h at 25°C and injected dorsally as described (Paré et al., 2014). After aging for ~2 h at 25°C, stage 7 embryos were washed with heptane, fixed in formaldehyde, and manually devitellinized for staining.

Cloning—See Table S1 for all primer sequences. The *pUASp-Toll-2-HA, pUASp-Toll-6-HA*, and *pUASp-Toll-8-HA* plasmids were previously described (Paré et al., 2014). All *tartan* and *Ten-m* constructs were generated by Gibson assembly with gel purified fragments (Illustra GFX Kit, GE) and ligated using NEBuilder HiFi DNA Assembly Master Mix (NEB). The *pUASp-tartan-HA* plasmid (containing a C-terminal 3× HA tag) was generated

by 2-part Gibson assembly. The *tartan* ORF was amplified from the GH10871 cDNA plasmid (Berkeley *Drosophila* Genome Project) with the primers tartan:HA Fwd and trn:HA Rev. The linearized backbone was generated by digesting *pUASp-W-CmR-ccdB-3xHA*, which contains a C-terminal 3×HA tag, with BamHI. The *pUASp-tartan–HA* transgene was inserted into the VK37 landing site on chromosome II. The *pUASp-HA–Ten-m* plasmid (containing an N-terminal 3× HA tag) was generated by 3-part Gibson assembly. The *Ten-m* ORF (RB isoform) was amplified in two parts from genomic DNA obtained from flies bearing a *UAS-Ten-m* transgene (Hong et al., 2012). The 5' end of the Ten-m open reading frame was amplified with primers Fwd N-3×HA:Tenm PB and Ten-m Rev_2. The 3' end of the *Ten-m* open reading frame was amplified using the primers Ten-m Fwd_2 and Rev N-3×HA:Ten-m PB. The linearized backbone was generated by digesting *pUASp-3xHA-W-CmR-ccdB* with MluI. The *Ten-m* open reading frame in this construct contains four polymorphisms that produce non-conservative amino acid changes at nucleotides 1513, 2108, 2978, and 6022 and a 109 nt microintron between the last two exons compared to the sequence on Flybase. The *pUASp-HA-Ten-m* transgene was inserted into the attP2 landing site on chromosome III.

The *pMT-tartan-AP5* and *pMT-AP5–Ten-m* plasmids expressing the Tartan ECD (amino acids 1–434) or the Ten-m ECD (amino acids 250–2,731) fused to alkaline phosphatase were cloned into the *pECIA14* expression vector (Özkan et al., 2013) using Gibson assembly. The *pMT-Toll-2-AP5*, *pMT-Toll-6-AP5*, and *pMT-Toll-8-AP5* plasmids were generated previously (Paré et al., 2014). The *pMT-tartan-AP5* plasmid was cloned by 2-part Gibson assembly. The tartan extracellular domain was amplified with Phusion polymerase from the GH10871 cDNA plasmid with the Fwd_Tartan_AP5 and Rev_Tartan_AP5 primers and cloned into the *pECIA14* backbone. The *pMT-AP5–Ten-m* plasmid was cloned by 3-part Gibson assembly. The Ten-m extracellular domain was amplified in two parts from *pUASp-HA–Ten-m*. The 5′ end of the Ten-m extracellular domain was amplified with the Fwd N-AP5_Ten-m and Ten-m Rev_2 primers. The 3′ end of the Ten-m extracellular domain was amplified with the Ten-m Fwd_2 and Rev N-AP5_Ten-m primers. A variant of *pECIA14* that contains an N-terminal AP5 tag was amplified with the Fwd N-AP5 PCR and Rev N-AP5 PCR primers.

Cell Culture Experiments and Analysis—The coding regions for the Tartan and Ten-m extracellular domains were cloned into the *pECIA14* expression vector (Addgene), which contains an inducible $CuSO_4$ promoter and a C-terminal human placental alkaline phosphatase gene Özkan et al., 2013). Constructs were transfected into *Drosophila* $S2R^+$ cells using FuGene HD Transfection Reagent (Promega, Southampton, UK), and protein expression was induced with 1 mM $CuSO_4$ 12 h post-transfection. Conditioned media was collected 2 days post-induction, concentrated for 30 min at 4,000 g using Amicon Ultra-4 Centrifugal Filter Units (100-kDa cutoff; Millipore), and stored at 4°C for use within 48 h. The same batch of concentrated media containing Tartan–AP5 or AP5–Ten-m was used for all conditions in each experiment.

Cells were transfected with *pActin5.1-Gal4* alone or in combination with *pUASp-Toll-2–HA, pUASp-Toll-6–HA, or pUASp-Toll-8–HA* (Paré et al., 2014), or *pUASp-tartan–HA* or *pUASp-HA–Ten-m* (this study). Plasmids were transfected at 300 ng/μl. Two days post-

transfection, cells were adhered to polylysine-coated coverslips for 2 h and washed with 1× PBS. Cells were then incubated 2 h with concentrated media from cells expressing pentameric alkaline phosphatase fusions diluted in Schneider's complete medium. Cells were washed once with 1× PBS, fixed 15 min in 4% formaldehyde/PBS, washed 3 times with 1× PBS, and blocked for 15 min in blocking buffer (1% BSA, 0.1% Triton, and 10 mM glycine). Cells were stained with rat anti-HA (1:500; Roche) and rabbit anti-human placental alkaline phosphatase (1:50; Thermo Fisher Scientific) primary antibodies and Alexa 488- and Alexa 647-conjugated secondary antibodies (1:500; Molecular Probes), mounted in ProLong Gold (Molecular Probes), and imaged using a Zeiss LSM700 confocal with a Plan-Apo 40×/1.3 NA oil-immersion objective. AP5 intensity at the plasma membrane of transfected and untransfected cells was quantified using the Freehand line tool in ImageJ (Figures 3B, 3E, 3F, and S3A–S3D). The multipoint tool in ImageJ was used to count cells with Ten-m or AP5 puncta (Figures 3C, 3D, 3G, and S3E–S3G).

For imaging endogenous Ten-m localization in $S2R^+$ cells, cells were transfected using FuGene HD Transfection Reagent (Promega) with *pActin5.1-Gal4* and *pUASp-tartan–HA* and mixed with untransfected cells two days post transfection. For cell aggregation experiments in cells transfected with *Ten-m* or control dsRNAs, $S2R^+$ cells were transfected with a cocktail of either (1) *pActin5.1-Gal4, pUASp-tartan–HA*, and *Toll-3* dsRNA, (2) *pActin5.1-Gal4, pUASp-tartan–HA*, and *Ten-m* dsRNA, (3) *pUASp-sqh–GFP*, empty *pUASp*, and *Toll-3* dsRNA, or (4) *pUASp-sqh*–GFP, empty *pUASp*, and *Ten-m* dsRNA. Plasmids and dsRNAs were transfected at 300 ng/μl. Cells were mixed in pairwise combinations two days post transfection. For both experiments, mixing was performed at 60 rpm for 30 min at room temperature, and cells were then adhered to polylysine-coated coverslips for 2 h and washed with 1× PBS. Cells were fixed in 4% formaldehyde/PBS for 15 min, washed 3 times with 1× PBS, blocked 30 min in blocking buffer as above, and stained with mouse anti-Ten-m (1:500) (Levine et al., 1994), rabbit anti-HA (1:500) (Cell Signaling), chicken anti-GFP (1:500) (Abcam) primary antibodies and Alexa 488-, Alexa 546-, and Alexa 647-conjugated secondary antibodies (1:500; Molecular Probes), mounted in ProLong Gold (Molecular Probes), and imaged on a Zeiss LSM700 confocal with a Plan-Apo 403/1.3 NA oil-immersion objective.

Time-Lapse Imaging—Movies were acquired as described (Paré et al., 2014). Embryos expressing Spider–GFP were imaged on a PerkinElmer Ultraview VOX spinning-disk confocal microscope with a Plan-Neo40×/1.3 NA oil-immersion objective (Zeiss) using Volocity acquisition software. Image stacks were acquired at 1.0-μm z-steps and 15-s intervals. Apical planes in the region of the adherens junctions were projected using tools for semi-automated image segmentation using SEGGA software (Farrell et al., 2017).

Western Blots—Western blots were performed on ~100 μl $S2R^+$ cells/lane or 10 embryos/lane (hand-selected by stage, punctured with a glass needle, and boiled in 20 μl 1× SDS buffer) run on a bis-Tris 4%–12% acrylamide NuPage gel (Invitrogen), transferred to a PVDF membrane (Millipore), and immunoblotted with mouse anti-Ten-m (1:1000) (Levine et al., 1994) or mouse anti-β-catenin (1:500) (Riggleman et al., 1990). Bands were detected using HRP-conjugated secondary antibodies (Jackson Laboratory) and chemiluminescence

with the Amersham ECL prime reagent (GE Healthcare). Bands were imaged on a Fujifilm LAS-3000 imager.

***Toll-2^{attP}* Allele—**The *Toll-2*^{attP} null mutation was generated by injection of *in vitro* synthesized guide RNAs (gRNAs) targeting the 5' and 3' UTRs of *Toll-2* with a donor containing *Toll-2* homology arms and an attP-DsRed-attP insert. gRNAs were generated using the T7 Megascript kit (Ambion) from PCR templates (Bassett et al., 2013) amplified with primers ZKM100 for the 5' cut or ZKM101 for the 3′ cut and the universal reverse primer ZKM002. The *Toll-2* attP donor construct was cloned according to Zhang et al. (Zhang et al., 2014). Homology arms of 1.2 kb (left) and 1 kb (right) were amplified using primers ZKM102/ZKM103 (left) and ZKM104/ZKM105 (right) and cloned into the *pJET* vector. The two gRNAs were co-injected with the donor construct into *act-Cas9, DNAlig4*^{169} embryos (65 ng/µl each gRNA and 500 ng/µl donor in H_2O). Injections were carried out as described (Paré et al., 2014). Injected embryos were aged for 48 h at 18°C and the larvae were transferred to food vials at room temperature. Adults with mosaic DsRed eyes were crossed to *Sp/CyO* flies, and the larval progeny were screened for DsRed expression in the nervous system. DsRed expression was confirmed by fluorescence in the adult eye and by PCR with primers ZKM027 and ZKM028. Candidate male flies were crossed to *Sp/CyO* females and then processed for genomic DNA isolation. The landing site was confirmed by PCR by pairing primers outside of the homology arms with primers inside the STOP-DsRed cassette (ZKM059 with ZKM028 for the left side and ZKM060 with ZKM027 for the right side). We confirmed the absence of the pBS backbone from the gDNA using primers ZKM013 and ZKM014. The absence of *Toll-2* expression was confirmed by *in situ* hybridization.

***Toll-6^{attP}* Allele—**The *Toll-6*^{attP} null mutation was generated by crossing flies harboring a transgenic plasmid expressing two gRNAs targeting the 5' UTR and the intergenic region downstream of *Toll-6* (*pCFD4-Toll-6*) to *nanos-Cas9* flies and injecting their progeny with a donor attP construct containing *Toll-6* left and right homology arms flanking an attP-DsRed-attP insert (Port et al., 2015). The *pCFD4Toll-6* gRNA plasmid was cloned according to crisprflydesign.org and (Port et al., 2015) by 2-part Gibson assembly of BbsI-digested *pCFD4* with a gel-purified PCR product amplified from *pCFD4* with the ZKM147 and ZKM149 primers (NEBuilder HiFi 23 Master Mix, NEB) and inserted into attP40. The *Toll-6*-attP donor construct was cloned according to Zhang et al. (Zhang et al., 2014). Homology arms of ~1 kb were amplified using primers ZKM128/ZKM130 (left) and ZKM135/ZKM138 (right), cloned into the *pJET* vector, and assembled using Golden Gate assembly. Injections were carried out as described above. Donor insertion was screened by DsRed fluorescence in the adult eye and larval nervous system and verified by PCR with pairing primers outside of the homology arms and primers within the attP-DsRed-attP cassette (ZKM139 with ZKM028 for the left side and ZKM027 with ZKM140 for the right side). The absence of *Toll-6* expression was confirmed by *in situ* hybridization.

***Toll-8$^{\Delta 6B}$* Deletion Allele—**The *pCFD4-Toll-8* gRNA plasmid was cloned according to the crisprflydesign.org protocol by 2-part Gibson assembly of BbsI-digested pCFD4 with a gel-purified PCR product amplified from *pCFD4* with the ZKM203 and ZKM205 primers

(NEBuilder HiFi 23 Master Mix, NEB). This plasmid was injected (250 ng/μl) into the embryos of *nanos-Cas9/+/Y; Toll-6*^{attP}/+ parents. Progeny were confirmed after crossing using primers spanning the *Toll-8* locus. The absence of *Toll-8* expression was confirmed by *in situ* hybridization.

***tartan* Deletion Alleles—**The *pCFD4-tartan* gRNA plasmid was cloned according to the crisprflydesign.org protocol by 2-part Gibson assembly of BbsI-digested pCFD4 with a gel-purified PCR product amplified from *pCFD4* with the ZKM272 and ZKM273 primers. This plasmid was injected (250 ng/μl) into *nanos-Cas9/+/Y; Toll-8*$^{\Delta 6B}$, *Toll-6*^{attP}/+ embryos and resulting adults were crossed to *Dr/TM3* females. The male progeny of injected flies that were w/Y; *trn*/TM3 or *w/Y*; *trn*, *Toll-8*$^{\Delta 6B}$, *Toll-6*^{attP}/*TM3* were genotyped by PCR after crossing to *Dr/TM3* females. Stable lines were generated, the absence of *pCFD4-trn* was determined by PCR, and the presence of *trn* deletions in both single and triple mutants was confirmed by PCR using primers spanning the deletion. The presence of the *Toll-6*^{attP} mutation in the triple mutant was confirmed by the presence of DsRed fluorescence in the eye and by PCR (above), and the absence of *tartan* and *Toll-8* expression in the triple mutant was confirmed by *in situ* hybridization. The absence of *tartan* expression in the *tartan* single mutant was confirmed by *in situ* hybridization and by the absence of staining with the guinea pig anti-Tartan antibody (Mao et al., 2008).

QUANTIFICATION AND STATISTICAL ANALYSIS

Specific n values and statistical analyses can be found in the Figure legends. Statistical analyses were performed in Prism 7 (GraphPad). For all early embryo analyses, ventrolateral cells in parasegments 3–6 were analyzed. To score myosin cables during convergent extension, five compartment boundaries per embryo were scored for the presence of myosin cables (defined as strong myosin accumulation at three or more consecutive vertical edges). We found that dorsal injection resulted in an additional, subtle defect in myosin cable formation at non-boundary edges in *Ten-m* KD (Figures 4C and 4D), *Ten-m* KD2 (Figures S5C and S5D), and *tartan* dsRNA-injected embryos (not shown). As myosin defects at non-boundary edges were not observed in *tartan* null mutants (Figures 2C and 2D), we speculate that these defects are due to effects of the injection protocol and may not reflect a true non-boundary role for Tartan or Ten-m. For the analysis of myosin recruitment in stage 15 embryos, the average intensity of myosin–GFP at the anterior boundary of 2–5 *engrailed* stripes per embryo was measured in ImageJ and normalized to the average intensity of the smooth cell region between the *engrailed* stripes.

Par-3 images were maximum intensity projections of z-planes encompassing the region of the adherens junctions in early stage 7 embryos. For Par-3 planar cell polarity measurements, cell boundaries were segmented and manually corrected using SEGGA software (Farrell et al., 2017). Background signal was subtracted based on the cytoplasmic intensities of the 20 closest cells as described (Farrell et al., 2017), and the $\log_2$ ratio of Par-3 intensity at vertical edges (edges oriented 60–90° to the AP axis) relative to horizontal edges (0–30°) was calculated for individual cells. Cells without at least one edge in each category were not analyzed. Cells were assigned to columns based on costaining with a *wg* mRNA probe or Wg antibody (columns 4 and 8). Cells immediately posterior to

Wgexpressing cells were assigned as columns 5 and 1. Columns 2/3 and 6/7 were combined for analysis; some parasegments contained only three cells (Tetley et al., 2016). Even and odd parasegments were assigned based on proximity to the cephalic furrow (parasegment 1). A single mean $\log_2$ ratio was calculated for each column in each embryo, the mean values were converted to absolute ratios, and the mean±SEM between embryos was plotted.

For Par-3 edge polarity measurements, cell edges within or between columns were manually selected and intensity values were measured using SIESTA software (Fernandez-Gonzalez and Zallen, 2011). Lines were manually drawn along cell interfaces, avoiding vertices. Vertical edges were defined as interfaces oriented 70–90° relative to the AP axis and were assigned as boundary or non-boundary edges based on position. Horizontal edges were defined as all edges located within columns, regardless of angle. Background signal was first subtracted based on the average cytoplasmic intensity of 20 randomly selected cells, and edge polarity was calculated as the inverse value of Par-3 fluorescence intensity at vertical edges relative to all horizontal edges. A single average value was calculated for all boundary edges and all non-boundary edges in each embryo, and the mean±SEM between embryos was plotted.

For the analysis of edge contraction events and tissue elongation, images were segmented using SEGGA software (Farrell et al., 2017). All cells that could be tracked for at least 50 time points (12.5 min) after t=0 were included in the edge contraction analysis, and all cells that could be tracked for 30 min after t=0 were used for the tissue elongation analysis, as described previously (Farrell et al., 2017). For the analysis of intercalation errors, edges that were close to vertical in early stage 7 were manually tracked for 30 min or until the time of edge disappearance (100 edges/embryo). Errors were scored as ‘no contraction’ (edge was still present after 30 min), ‘no vertex resolution’ (edge contracted to a vertex that did not resolve after 10 min), ‘unstable new edge’ (edge contracted to a vertex and formed a new horizontal edge, but this edge subsequently contracted back to a vertex), and ‘incorrect orientation of new edge’ (edge contracted to a vertex that resolved to reform the original vertical edge).

DATA AND CODE AVAILABILITY

No large-scale datasets or new code were generated in this study.

Supplementary Material

Refer to Web version on PubMed Central for supplementary material.

ACKNOWLEDGMENTS

We thank Maria Bustillo for many valuable discussions and for the initial observation that Ten-m localizes to compartment boundaries, Omar Gutierrez-Ruiz for cloning assistance, Kia Bourdot and Sara Supriyatno for help with time-lapse imaging, Nicole Guillery and Tarek Islam for help with image segmentation and analysis, and Wilaysha Evans for help with embryo collections. We are grateful to Ron Wides for the Ten-m antibody, Allen Laughon, Clemence Levet, and Matthew Freeman for the Tartan antibodies, and Richard Zallen, Mimi Shirasu-Hiza, and members of the Zallen lab for helpful discussions and comments on the manuscript. This work was funded by NIH R01 grant GM079340 to J.A.Z. J.S. is supported by NIH/NCI F30 grant CA236441–01 and is a student of the Weill Cornell/Rockefeller/Sloan Kettering Tri-Institutional MD-PhD program, which is supported by NIH/NIGMS T32 grant GM007739. J.A.Z. is an investigator of the Howard Hughes Medical Institute.

REFERENCES

Antinucci P, Nikolaou N, Meyer MP, and Hindges R. (2013). Teneurin-3 specifies morphological and functional connectivity of retinal ganglion cells in the vertebrate visual system. Cell Rep. 5, 582–592. [PubMed: 24183672]

Bassett AR, Tibbit C, Ponting CP, and Liu JL (2013). Highly efficient targeted mutagenesis of *Drosophila* with the CRISPR/Cas9 system. Cell Rep. 4, 220–228. [PubMed: 23827738]

Batlle E, and Wilkinson DG (2012). Molecular mechanisms of cell segregation and boundary formation in development and tumorigenesis. Cold Spring Harb. Perspect. Biol. 4, a008227.

Baumgartner S, Martin D, Hagios C, and Chiquet-Ehrismann R. (1994). Tenm, a *Drosophila* gene related to tenascin, is a new pair-rule gene. EMBO J. 13, 3728–3740. [PubMed: 8070401]

Baumgartner S, and Wides R(2019). Discovery of teneurins. Front. Neurosci. 13, 230. [PubMed: 30941006]

Benton MA, Pechmann M, Frey N, Stappert D, Conrads KH, Chen YT, Stamataki E, Pavlopoulos A, and Roth S. (2016). Toll genes have an ancestral role in axis elongation. Curr. Biol. 26, 1609–1615. [PubMed: 27212406]

Berns DS, DeNardo LA, Pederick DT, and Luo L. (2018). Teneurin-3 controls topographic circuit assembly in the hippocampus. Nature554, 328–333. [PubMed: 29414938]

Bertet C, Sulak L, and Lecuit T. (2004). Myosin-dependent junction remodelling controls planar cell intercalation and axis elongation. Nature429, 667–671. [PubMed: 15190355]

Bielmeier C, Alt S, Weichselberger V, La Fortezza M, Harz H, Jülicher F, Salbreux G, and Classen AK (2016). Interface contractility between differently fated cells drives cell elimination and cyst formation. Curr. Biol. 26, 563–574. [PubMed: 26853359]

Blankenship JT, Backovic ST, Sanny JS, Weitz O, and Zallen JA (2006). Multicellular rosette formation links planar cell polarity to tissue morphogenesis. Dev. Cell 11, 459–470. [PubMed: 17011486]

Boucard AA, Maxeiner S, and Su€dhof TC (2014). Latrophilins function as heterophilic cell-adhesion molecules by binding to teneurins: regulation by alternative splicing. J. Biol. Chem. 289, 387–402. [PubMed: 24273166]

Brennan CA, and Anderson KV (2004). *Drosophila*: the genetics of innate immune recognition and response. Annu. Rev. Immunol. 22, 457–483. [PubMed: 15032585]

Brook WJ, and Cohen SM (1996). Antagonistic interactions between wingless and decapentaplegic responsible for dorsal-ventral pattern in the *Drosophila* leg. Science 273, 1373–1377. [PubMed: 8703069]

Calzolari S, Terriente J, and Pujades C. (2014). Cell segregation in the vertebrate hindbrain relies on actomyosin cables located at the interhombomeric boundaries. EMBO J. 33, 686–701. [PubMed: 24569501]

Carvalho L, Jacinto A, and Matova N. (2014). The Toll/NF-kB signaling pathway is required for epidermal wound repair in *Drosophila*. Proc. Natl. Acad. Sci. USA111, E5373–E5382. [PubMed: 25427801]

Chang Z, Price BD, Bockheim S, Boedigheimer MJ, Smith R, and Laughon A. (1993). Molecular and genetic characterization of the *Drosophila tartan* gene. Dev. Biol. 160, 315–332. [PubMed: 8253267]

Dahmann C, Oates AC, and Brand M. (2011). Boundary formation and maintenance in tissue development. Nat. Rev. Genet. 12, 43–55. [PubMed: 21164524]

de Wit J, Hong W, Luo L, and Ghosh A. (2011). Role of leucine-rich repeat proteins in the development and function of neural circuits. Annu. Rev. Cell Dev. Biol. 27, 697–729. [PubMed: 21740233]

del Álamo D, Rouault H, and Schweisguth F. (2011). Mechanism and significance of cis-inhibition in Notch signaling. Curr. Biol. 21, R40–R47. [PubMed: 21215938]

Dharmaratne N, Glendining KA, Young TR, Tran H, Sawatari A, and Leamey CA (2012). Ten-m3 is required for the development of topography in the ipsilateral retinocollicular pathway. PLoS One 7, e43083.

Dolan J, Walshe K, Alsbury S, Hokamp K, O'Keeffe S, Okafuji T, Miller SF, Tear G, and Mitchell KJ (2007). The extracellular leucine-rich repeat superfamily: a comparative survey and analysis of evolutionary relationships and expression patterns. BMC Genomics 8, 320. [PubMed: 17868438]

Drabikowski K, Trzebiatowska A, and Chiquet-Ehrismann R. (2005). An essential gene for germ cell development, epidermal morphogenesis, gonad migration, and neural pathfinding in *Caenorhabditis elegans*. Dev. Biol. 282, 27–38. [PubMed: 15936327]

Fagotto F, Rohani N, Touret AS, and Li R. (2013). A molecular base for cell sorting at embryonic boundaries: contact inhibition of cadherin adhesion by ephrin/Eph-dependent contractility. Dev. Cell27, 72–87. [PubMed: 24094740]

Farrell DL, Weitz O, Magnasco MO, and Zallen JA (2017). SEGGA: a toolset for rapid automated analysis of epithelial cell polarity and dynamics. Development 144, 1725–1734. [PubMed: 28465336]

Fernandez-Gonzalez R, and Zallen JA (2011). Oscillatory behaviors and hierarchical assembly of contractile structures in intercalating cells. Phys. Biol. 8, 045005.

Galea GL, Cho YJ, Galea G, Mole MA, Rolo A, Savery D, Moulding D, Culshaw LH, Nikolopoulou E, Greene NDE, et al. (2017). Biomechanical coupling facilitates spinal neural closure in mouse embryos. Proc. Natl. Acad. Sci. USA 114, E5177–E5186. [PubMed: 28607062]

Garcia-Bellido A, Ripoll P, and Morata G. (1973). Developmental compartmentalisation of the wing disk of *Drosophila*. Nat. New Biol. 245, 251–253. [PubMed: 4518369]

Hong W, Mosca TJ, and Luo L. (2012). Teneurins instruct synaptic partner matching in an olfactory map. Nature484, 201–207. [PubMed: 22425994]

Hong W, Zhu H, Potter CJ, Barsh G, Kurusu M, Zinn K, and Luo L. (2009). Leucine-rich repeat transmembrane proteins intstruct discrete dendrite targeting in an olfactory map. Nat. Neurosci. 12, 1542–1550. [PubMed: 19915565]

Horn T, and Boutros M. (2010). E-RNAi: a web application for the multi-species design of RNAi reagents—2010 update. Nucleic Acids Res. 38, W332–W339. [PubMed: 20444868]

Huebner RJ, and Wallingford JB (2018). Coming to consensus: a unifying model emerges for convergent extension. Dev. Cell 46, 389–396. [PubMed: 30130529]

Irvine KD, and Wieschaus E. (1994). Cell intercalation during *Drosophila* germband extension and its regulation by pair-rule segmentation genes. Development120, 827–841. [PubMed: 7600960]

Kinel-Tahan Y, Weiss H, Dgany O, Levine A, and Wides R. (2007). *Drosophila* odz gene is required for multiple cell types in the compound retina. Dev. Dyn. 236, 2541–2554. [PubMed: 17685476]

Kleve CD, Siler DA, Syed SK, and Eldon ED (2006). Expression of 18wheeler in the follicle cell epithelium affects cell migration and egg morphology in Drosophila. Dev. Dyn. 235, 1953–1961. [PubMed: 16607637]

Kolesnikov T, and Beckendorf SK (2007). 18 Wheeler regulates apical constriction of salivary gland cells vis the Rho-GTPase-signaling pathway. Dev. Biol. 307, 53–61. [PubMed: 17512518]

Krause C, Wolf C, Hemphala J, Samakovlis C, and Schuh R. (2006). Distinct functions of the leucine-rich repeat transmembrane proteins capricious and tartan in the *Drosophila* tracheal morphogenesis. Dev. Biol. 296, 253–264. [PubMed: 16764850]

Kurusu M, Cording A, Taniguchi M, Menon K, Suzuki E, and Zinn K. (2008). A screen of cell-surface molecules identifies leucine-rich repeat proteins as key mediators of synapic target selection. Neuron59, 972–985. [PubMed: 18817735]

Landsberg KP, Farhadifar R, Ranft J, Umetsu D, Widmann TJ, Bittig T, Said A, Julicher F, and Dahmann C. (2009). Increased cell bond tension governs cell sorting at the *Drosophila* anterioposterior compartment boundary. Curr. Biol. 19, 1950–1955. [PubMed: 19879142]

Larsen C, Bardet PL, Vincent JP, and Alexandre C. (2008). Specification and positioning of parasegment grooves in *Drosophila*. Dev. Biol. 321, 310–318. [PubMed: 18692780]

Lawrence PA, and Struhl G. (1996). Morphogens, compartments, and pattern: lessons from *Drosophila*?Cell85, 951–961. [PubMed: 8674123]

Leamey CA, Merlin S, Lattouf P, Sawatari A, Zhou X, Demel N, Glendining KA, Oohashi T, Sur M, and Fassler R. (2007). Ten-m3 regulates eye-specific patterning in the mammalian visual pathway and is required for binocular vision. PLoS Biol. 5, e241.

Levine A, Bashan-Ahrend A, Budai-Hadrian O, Gartenberg D, Menasherow S, and Wides R. (1994). Odd Oz: a novel *Drosophila* pair rule gene. Cell77, 587–598. [PubMed: 7514504]

Lossie AC, Nakamura H, Thomas SE, and Justice MJ (2005). Mutation of I7Rn3 shows that Odz4 is required for mouse gastrulation. Genetics 169, 285–299. [PubMed: 15489520]

Ludwig MZ, Manu, Kittler R, White KP, and Kreitman M. (2011). Consequences of eukaryotic enhancer architecture for gene expression dynamics, development, and fitness. PLoS Genet. 7, e1002364.

Lye CM, Naylor HW, and Sanson B. (2014). Subcellular localisations of the CPTI collection of YFP-tagged proteins in *Drosophila* embryos. Development141, 4006–4017. [PubMed: 25294944]

Lye CM, and Sanson B. (2011). Tension and epithelial morphogenesis in *Drosophila* early embryos. Curr. Top. Dev. Biol. 95, 145–187. [PubMed: 21501751]

Major RJ, and Irvine KD (2005). Influence of Notch on dorsoventral compartmentalization and actin organization in the *Drosophila* wing. Development 132, 3823–3833. [PubMed: 16049109]

Major RJ, and Irvine KD (2006). Localization and requirement for myosin II at the dorsal-ventral compartment boundary of the *Drosophila* wing. Dev. Dyn. 235, 3051–3058. [PubMed: 17013876]

Mao Y, Kerr M, and Freeman M. (2008). Modulation of *Drosophila* retinal epithelial integrity by the adhesion proteins capricious and tartan. PLoS One3, e1827.

McIlroy G, Foldi I, Aurikko J, Wentzell JS, Lim MA, Fenton JC, Gay NJ, and Hidalgo A. (2013). Toll-6 and Toll-7 function as neurotrophin receptors in the *Drosophila melanogaster* CNS. Nat. Neurosci. 16, 1248–1256. [PubMed: 23892553]

Meyer SN, Amoyel M, Bergantiños C, de la Cova C, Schertel C, Basler K, and Johnston LA (2014). An ancient defense system eliminates unfit cells from developing tissues during cell competition. Science 346, 1258236.

Milan M, Párez L, and Cohen SM (2005). Boundary formation in the *Drosophila* wing: functional dissection of Capricious and Tartan. Dev. Dyn. 233, 804–810. [PubMed: 15830355]

Milan M, Weihe U, Perez L, and Cohen SM (2001). The LRR proteins Capricious and Tartan mediate cell interactions during DV boundary formation in the *Drosophila* wing. Cell 106, 785–794. [PubMed: 11572783]

Millard TH, and Martin P. (2008). Dynamic analysis of filopodia interactions during the zippering phase of *Drosophila* dorsal closure. Development135, 621–626. [PubMed: 18184725]

Monier B, Pélissier-Monier A, Brand AH, and Sanson B. (2010). An actomyosin-based barrier inhibits cell mixing at compartmental boundaries in *Drosophila* embryos. Nat. Cell Biol. 12, 60–69. [PubMed: 19966783]

Monier B, Pélissier-Monier A, and Sanson B. (2011). Establishment and maintenance of compartmental boundaries: role of contractile actomyosin barriers. Cell. Mol. Life Sci. 68, 1897–1910. [PubMed: 21437644]

Morisato D, and Anderson KV (1995). Signaling pathways that establish the dorsal-ventral pattern of the *Drosophila* embryo. Annu. Rev. Genet. 29, 371–399. [PubMed: 8825480]

Mosca TJ (2015). On the teneurin track: a new synaptic organization molecule emerges. Front. Cell. Neurosci. 9, 204. [PubMed: 26074772]

Mosca TJ, Hong W, Dani VS, Favaloro V, and Luo L. (2012). Trans-synaptic teneurin signalling in neuromuscular synapse organization and target choice. Nature484, 237–241. [PubMed: 22426000]

Ng A, Eisenberg J, Health R, Huett A, Robinson C, Nau G, and Xavier R. (2011). Human leucine-rich repeat proteins: a genome-wide bioinformatic categorization and functional analysis in innate immunity. Proc. Natl. Acad. Sci. USA108, 108.

Ninomiya H, Elinson RP, and Winklbauer R. (2004). Antero-posterior tissue polarity links mesoderm convergent extension to axial patterning. Nature430, 364–367. [PubMed: 15254540]

Nishimura M, Inoue Y, and Hayashi S. (2007). A wave of EGFR signaling determines cell alignment and intercalation in the *Drosophila* tracheal placode. Development134, 4273–4282. [PubMed: 17978004]

Oohashi T, Zhou XH, Feng K, Richter B, Morgelin M, Perez MT, Su WD, Chiquet-Ehrismann R, Rauch U, and Fassler R. (1999). Mouse tenm/Odz is a new family of dimeric type II transmembrane proteins expressed in many tissues. J. Cell Biol. 145, 563–577. [PubMed: 10225957]

Ozkan E, Carrillo RA, Eastman CL, Weiszmann R, Waghray D, Johnson KG, Zinn K, Celniker SE, and Garcia KC (2013). An extracellular interactome of immunoglobulin and LRR proteins reveals ligand-receptor networks. Cell 154, 228–239. [PubMed: 23827685]

Paré A, Lemons D, Kosman D, Beaver W, Freund Y, and McGinnis W. (2009). Visualization of individual Scr mRNAs during *Drosophila* embryogenesis yields evidence for transcriptional bursting. Curr. Biol. 19, 2037–2042. [PubMed: 19931455]

Paré AC, Vichas A, Fincher CT, Mirman Z, Farrell DL, Mainieri A, and Zallen JA (2014). A positional Toll receptor code directs convergent extension in *Drosophila*. Nature 515, 523–527. [PubMed: 25363762]

Peng Y, and Axelrod JD (2012). Asymmetric protein localization in planar cell polarity: mechanisms, puzzles, and challenges. Curr. Top. Dev. Biol. 101, 33–53. [PubMed: 23140624]

Port F, Muschalik N, and Bullock SL (2015). Systematic evaluation of *Drosophila* CRISPR tools reveals safe and robust alternatives to autonomous gene drives in basic research. G3 (Bethesda) 5, 1493–1502. [PubMed: 25999583]

Riggleman B, Schedl P, and Wieschaus E. (1990). Spatial expression of the *Drosophila* segment polarity gene armadillo is post-transcriptionally regulated by wingless. Cell63, 549–560. [PubMed: 2225066]

Royou A, Field C, Sisson JC, Sullivan W, and Karess R. (2004). Reassessing the role and dynamics of nonmuscle myosin II during furrow formation in early *Drosophila* embryos. Mol. Biol. Cell15, 838–850. [PubMed: 14657248]

Rubin BP, Tucker RP, Brown-Luedi M, Martin D, and Chiquet-Ehrismann R. (2002). Teneurin 2 is expressed by the neurons of the thalamofugal visual system *in situ* and promotes homophilic cell-cell adhesion *in vitro*. Development129, 4697–4705. [PubMed: 12361962]

Sakurai KT, Kojima T, Aigaki T, and Hayashi S. (2007). Differential control of cell affinity required for progression and refinement of cell boundary during *Drosophila* leg segmentation. Dev. Biol. 309, 126–136. [PubMed: 17655839]

Scarpa E, Finet C, Blanchard GB, and Sanson B. (2018). Actomyosindriven tension at compartmental boundaries orients cell division independently of cell geometry *in vivo*. Dev. Cell47, 727–740. [PubMed: 30503752]

Schneider CA, Rasband WS, and Eliceiri KW (2012). NIH Image to ImageJ: 25 years of image analysis. Nat. Methods 9, 671–675. [PubMed: 22930834]

Silva JP, Lelianova VG, Ermolyuk YS, Vysokov N, Hitchen PG, Berninghausen O, Rahman MA, Zangrandi A, Fidalgo S, Tonevitsky AG, et al. (2011). Latrophilin 1 and its endogenous ligand Lasso/teneurin-2 form a high-affinity transsynaptic receptor pair with signaling capabilities. Proc. Natl. Acad. Sci. USA 108, 12113–12118. [PubMed: 21724987]

Simoes S, Blankenship JT, Weitz O, Farrell DL, Tamada M, Fernandez-Gonzalez R, and Zallen JA (2010). Rho-kinase directs Bazooka/Par-3 planar polarity during *Drosophila* axis elongation. Dev. Cell 19, 377–388. [PubMed: 20833361]

Simoes S, Mainieri A, and Zallen JA (2014). Rho GTPase and Shroom direct planar polarized actomyosin contractility during convergent extension. J. Cell Biol. 204, 575–589. [PubMed: 24535826]

Sun J, Li L, Wang P, Zhang S, and Wu J. (2017b). Genome-wide characterization, evolution, and expression analysis of the leucine-rich repeat receptor-like protein kinase (LRR-RLK) gene family in *Rosaceae* genomes. BMC Genomics18, 763. [PubMed: 29017442]

Sun Z, Amourda C, Shagirov M, Hara Y, Saunders TE, and Toyama Y. (2017a). Basolateral protrusion and apical contraction cooperatively drive *Drosophila* germ-band extension. Nat. Cell Biol. 19, 375–383. [PubMed: 28346438]

Tetley RJ, Blanchard GB, Fletcher AG, Adams RJ, and Sanson B. (2016). Unipolar distributions of junctional myosin II identify cell stripe boundaries that drive cell intercalation throughout *Drosophila* axis extension. Elife5, e12094.

Tucker RP, Kenzelmann D, Trzebiatowska A, and Chiquet-Ehrismann R. (2007). Teneurins: transmembrane proteins with fundamental roles in development. Int. J. Biochem. Cell Biol. 39, 292–297. [PubMed: 17095284]

Umetsu D, Aigouy B, Aliee M, Sui L, Eaton S, Jülicher F, and Dahmann C. (2014). Local increases in mechanical tension shape compartment boundaries by biasing cell intercalations. Curr. Biol. 24, 1798–1805. [PubMed: 25065753]

Urbano JM, Naylor HW, Scarpa E, Muresan L, and Sanson B. (2018). Suppression of epithelial folding at actomyosin-enriched compartment boundaries downstream of Wingless signalling in *Drosophila*. Development145, 1–13.

Vincent JP, and O'Farrell PH (1992). The state of engrailed expression is not clonally transmitted during early *Drosophila* development. Cell 68, 923–931. [PubMed: 1547492]

Ward A, Hong W, Favaloro V, and Luo L. (2015). Toll receptors instruct axon and dendrite targeting and participate in synaptic partner matching in a *Drosophila* olfactory circuit. Neuron85, 1013–1028. [PubMed: 25741726]

Yagi Y, Nishida Y, and Ip YT (2010). Functional analysis of Toll-related genes in Drosophila. Dev. Growth Differ. 52, 771–783. [PubMed: 21158756]

Yang Y, and Mlodzik M. (2015). Wnt-Frizzled/planar cell polarity signaling: cellular orientation by facing the Wind (Wnt). Annu. Rev. Cell Dev. Biol. 31, 623–646. [PubMed: 26566118]

Zallen JA (2007). Planar polarity and tissue morphogenesis. Cell 129, 1051–1063. [PubMed: 17574020]

Zallen JA, and Blankenship JT (2008). Multicellular dynamics during epithelial elongation. Semin. Cell Dev. Biol. 19, 263–270. [PubMed: 18343171]

Zallen JA, and Wieschaus E. (2004). Patterned gene expression directs bipolar planar polarity in *Drosophila*. Dev. Cell6, 343–355. [PubMed: 15030758]

Zhang S, Amourda C, Garfield D, and Saunders TE (2018). Selective filopodia adhesion ensures robust cell matching in the *Drosophila* heart. Dev. Cell 46, 189–203.e4.

Zhang X, Koolhaas WH, and Schnorrer F. (2014). A versatile two-step CRISPR- and RMCE-based strategy for efficient genome engineering in *Drosophila*. G3 (Bethesda)4, 2409–2418. [PubMed: 25324299]

Zheng L, Michelson Y, Freger V, Avraham Z, Venken KJ, Bellen HJ, Justice MJ, and Wides R. (2011). *Drosophila* ten-m and filamin affect motor neuron growth cone guidance. PLoS One6, e22956.

Zipursky SL, and Sanes JR (2010). Chemoaffinity revisited: Dscams, Protocadherins, and neural circuit assembly. Cell 143, 343–353. [PubMed: 21029858]

Highlights

- Tartan and Ten-m receptors direct planar polarity at compartment boundaries
- Striped Tartan expression sets the position of compartment boundaries
- Tartan recruits Ten-m *in trans* and inhibits its membrane localization *in cis*
- Differences in Tartan and Ten-m levels are essential for boundary structure

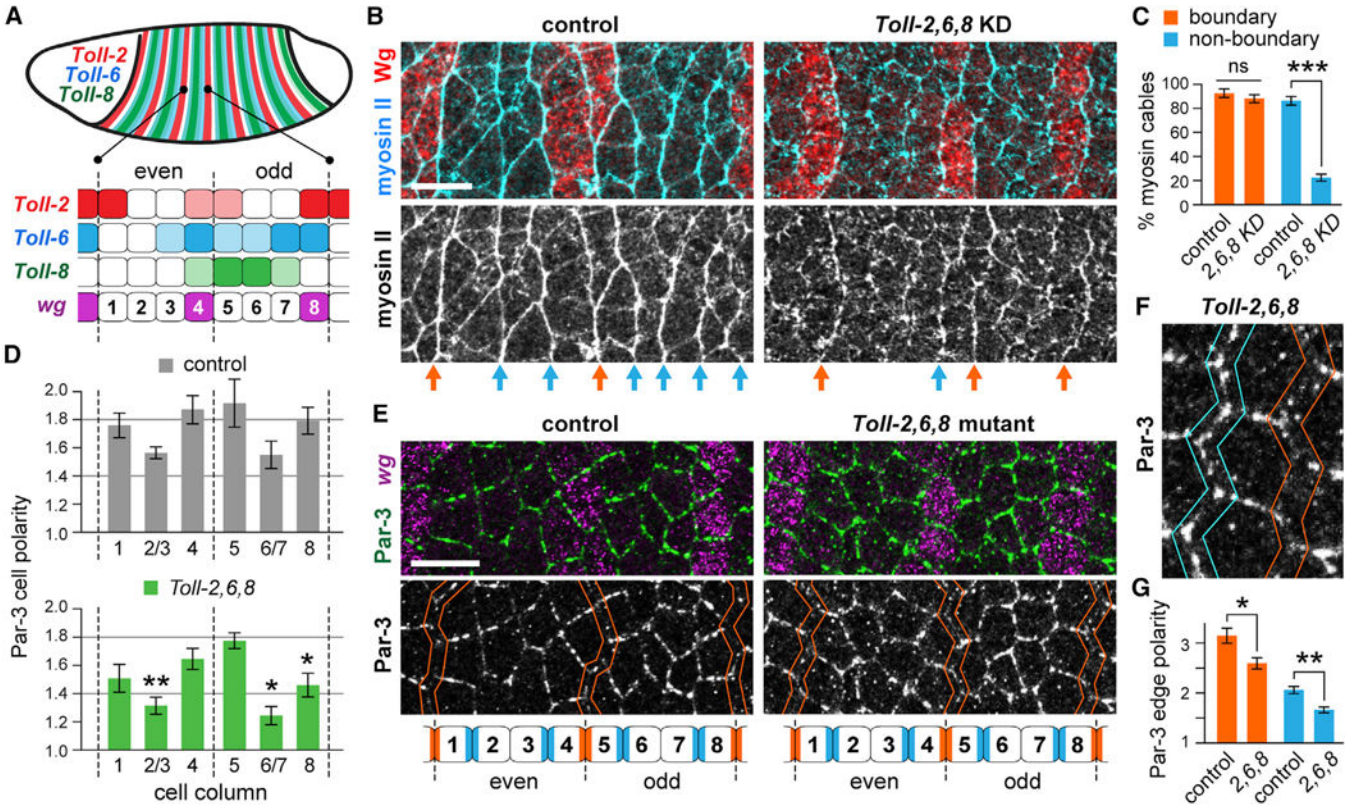

Figure 1. Compartment Boundaries Display Planar Polarity in the Absence of Toll-2, Toll-6, and Toll-8

(A) *Toll*-2, *Toll*-6, and *Toll*-8 are expressed in repeating two-compartment units along the anterior-posterior axis. Compartment boundaries, dashed lines.

(B) Myosin–GFP and Wg proteins in control and *Toll-2,6,8* KD embryos. Arrows, myosin cables. Compartment boundaries, orange. Non-boundary interfaces, cyan.

(C) Percentage of boundaries and non-boundary interfaces with myosin cables in control and *Toll-2,6,8* KD embryos.

(D) Par-3 planar cell polarity was reduced in some columns in *Toll-2,6,8* mutant embryos compared with controls.

(E) Par-3 protein and *wg* mRNA in control and *Toll-2,6,8* mutants.

(F) Close-up of Par-3 at the 8/1 compartment boundary (orange) and the 7/8 non-boundary interface (cyan) in the *Toll-2,6,8* mutant in (E).

(G) Par-3 edge polarity (the inverse ratio of Par-3 intensity at vertical boundary or non-boundary edges relative to horizontal edges) in control and *Toll-2,6,8* mutants.

A single average was calculated for each embryo and the mean ± SEM between embryos is shown. *p ≤ 0.02, **p < 0.005, ***p < 0.0001, two-tailed Student's t test. n = 8–10 late stage 7 embryos per genotype in (C) (3–5 boundaries and 4–13 non-boundaries per embryo), 7 early stage 7 embryos per genotype in (D) (10–44 cells per column in each embryo), and 7 early stage 7 embryos in (G) (33–59 boundary edges and 68–122 non-boundary edges per embryo). Genotypes: control in (B) and (C) (myosin–GFP, $Toll\text{-}8^{59/+}$ injected with water), *Toll-2,6,8* KD (myosin–GFP, $Toll\text{-}8^{59/145}$ injected with *Toll-2* and *Toll-6* dsRNAs), control in (D)– (G) ($Toll\text{-}2^{attP}$/+ or +/+; $Toll\text{-}8^{\Delta 6B}$, $Toll\text{-}6^{attP}$/+ or +/+); *Toll-2,6,8* mutant ($Toll\text{-}2^{attP}$;

Toll-8$^{\Delta 6B}$, *Toll-6*^{attP}). Embryos are late stage 7 in (B) and early stage 7 in (E) and (F). Anterior left, dorsal up. Bars, 10 μm. See also Figures S1 and S2.

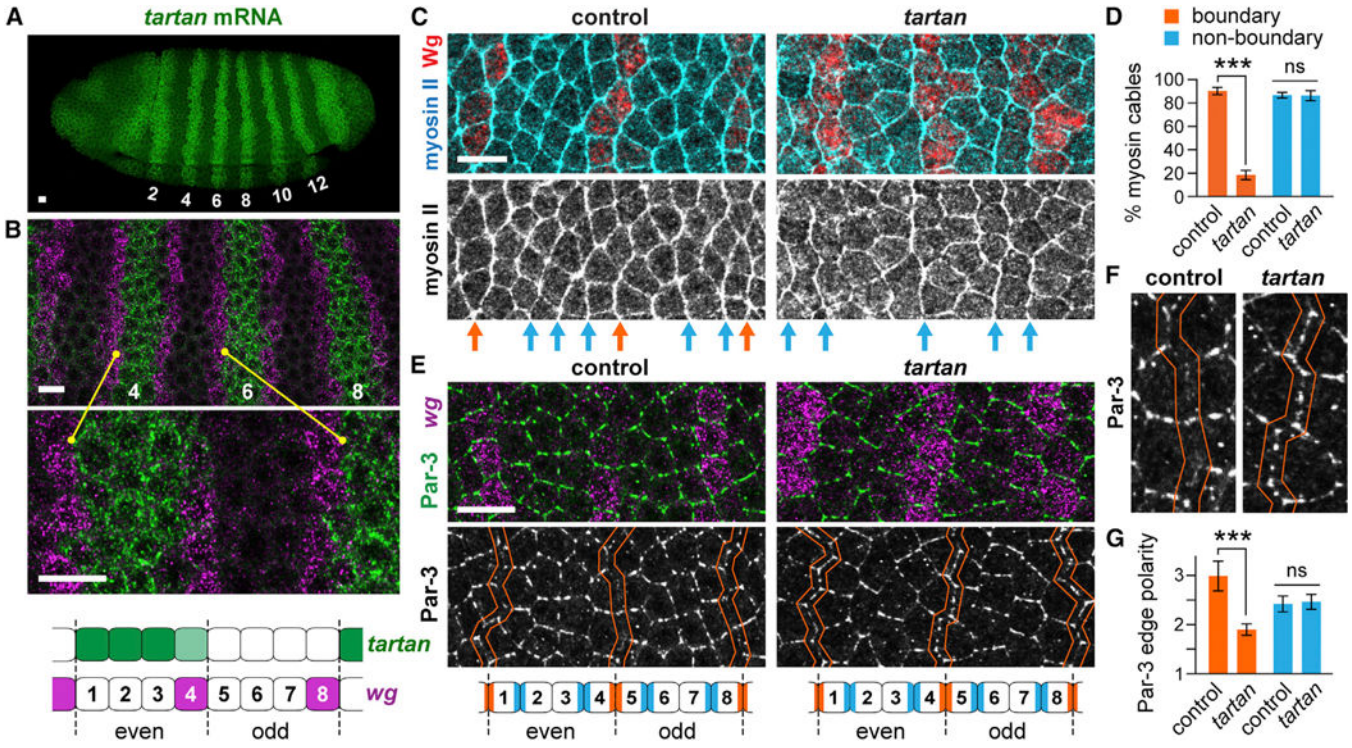

Figure 2. The Striped Receptor Tartan Regulates Planar Polarity at Compartment Boundaries

(A and B) *tartan* mRNA expression prior to (A) and during (B) convergent extension. Even compartments are indicated.

(C) Myosin–GFP and Wg proteins in control and *tartan* mutant embryos. Arrows, myosin cables. Compartment boundaries, orange. Non-boundary interfaces, cyan.

(D) Percentage of boundaries and non-boundary interfaces with myosin cables in control and *tartan* mutant embryos.

(E) Par-3 protein and wg mRNA in control and *tartan* mutant embryos.

(F) Close-up of Par-3 at the 4/5 compartment boundaries in (E).

(G) Par-3 edge polarity at boundary and non-boundary edges in control and *tartan* mutant embryos.

A single average was calculated for each embryo and the mean ± SEM between embryos is shown. ***$p < 0.0001$, two-tailed Student's t test. n = 9–11 late stage 7 embryos per genotype in (D) (3–5 boundaries and 5–12 non-boundaries per embryo) and 7 early stage 7 embryos per genotype in (G) (33–55 boundary edges and 64–108 non-boundary edges per embryo). Genotypes: control in (C) and (D) (myosin–GFP/+; trn^{3C}/+ or +/+), *tartan* in (C) and (D) (myosin–GFP/+; trn^{3C}), control in (E)–(G) (trn^{3C}/+ or +/+); *tartan* in (E)–(G) (trn^{3C}). Embryos are stage 6 in (A), early stage 7 in (B), (E), and (F), and late stage 7 in (C). Anterior left, dorsal up. Bars, 10 μm. See also Figure S2.

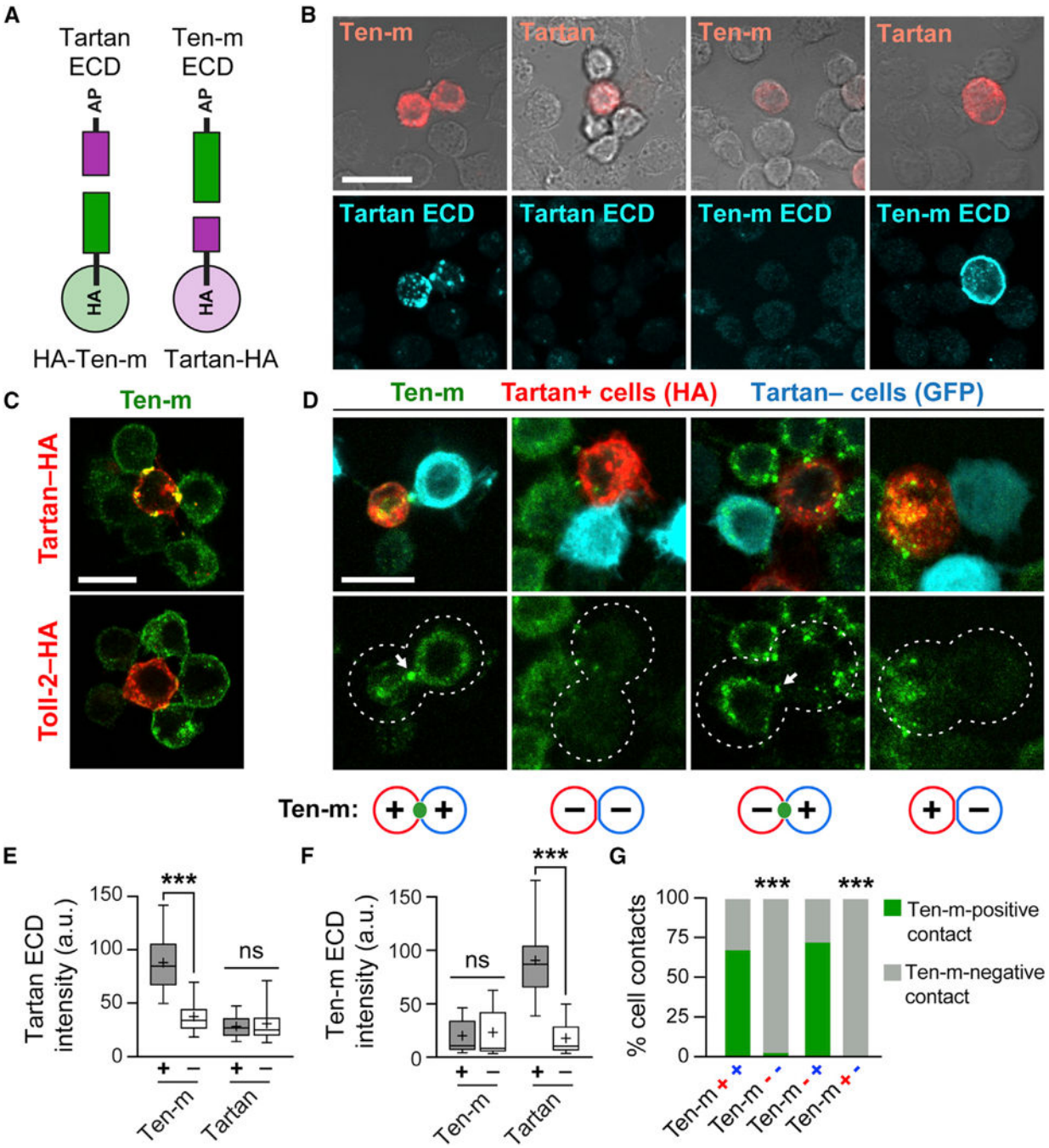

Figure 3. Tartan Interacts with the Teneurin Ten-m *in vitro*

(A) *Drosophila* S2R$^+$ cells expressing full-length HA-tagged receptors were tested for binding to the extracellular domains (ECDs) of Tartan and Ten-m.

(B) Tartan ECD (left panels) binds to S2R$^+$ cells expressing HA–Ten-m but not Tartan–HA. Ten-m ECD (right panels) binds to S2R$^+$ cells expressing Tartan–HA but not HA–Ten-m. ECDs were visualized with antibodies to alkaline phosphatase (AP), receptor-expressing cells were labeled with antibodies to HA.

(C) Endogenous Ten-m protein in $S2R^+$ cells is recruited to sites of contact with cells that express Tartan–HA (68.4% of cells, n = 291) (top), but not cells that express Toll-2–HA (7.1%, n = 126) (bottom) or Toll-8–HA (8.3%, n = 180) (not shown) ($p < 0.0001$ for Tartan–HA versus Toll-2–HA or Toll-8–HA, χ^2 test).

(D) Ten-m accumulation at interfaces between Tartan–HA-expressing and non-expressing cells was not affected by *Ten-m* KD (−) in the Tartan–HA-expressing (Tartan+) cells (labeled with antibodies to HA), but was eliminated by *Ten-m* KD in Tartan–HA-non-expressing cells (visualized by transfection with myosin–GFP). Cells were transfected with *Ten-m* dsRNA (*Ten-m-*) or control *Toll-3* dsRNA (*Ten-m+*).

(E and F) Tartan ECD or Ten-m ECD intensity at the surface of cells expressing the indicated receptors (+) versus untransfected controls (−). Boxes, 25^{th}–75^{th} percentile; whiskers, 5^{th}–95^{th} percentile; horizontal line, median; +, mean. ***$p < 0.0001$, one-way ANOVA with Sidak's multiple comparisons test including additional conditions (see Figure S3). n = 50–95 untransfected cells and 120–241 transfected cells in 2–4 independent experiments.

(G) Percentage of interfaces with Ten-m accumulation in (D). ***$p < 0.0001$ versus ++, χ^2 test. n = 31–40-cell pairs analyzed for each combination. Bars, 10 μm.

See also Figures S3 and S4.

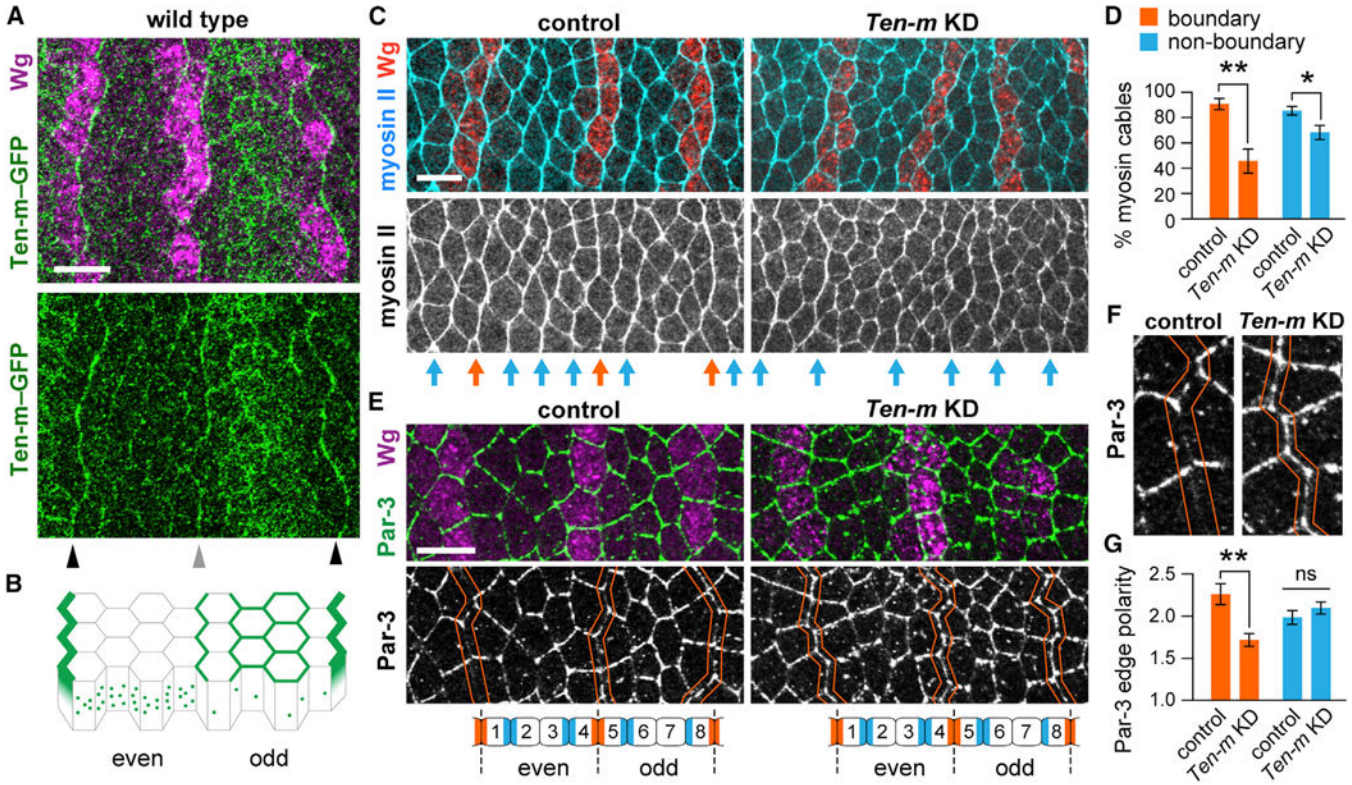

Figure 4. Ten-m Localizes to Compartment Boundaries and Is Required for Boundary Polarity

(A) Ten-m–GFP localization (apical plane) relative to Wingless (Wg). Ten-m–GFP localizes strongly to the 8/1 compartment boundary (black arrowheads), weakly to the 4/5 compartment boundary (gray arrowhead), and to the apical membrane of cells in odd compartments.

(B) Schematic of Ten-m localization.

(C) Myosin–GFP and Wg proteins in control (water-injected) and *Ten-m* KD (*Ten-m* dsRNA-injected) embryos. Arrows, myosin cables. Compartment boundaries, orange. Non-boundary interfaces, cyan.

(D) Percentage of boundaries and non-boundary interfaces with myosin cables in control and *Ten-m* KD embryos.

(E) Par-3 and Wg proteins in control and *Ten-m* KD embryos.

(F) Close-up of Par-3 at the 8/1 compartment boundaries in (E).

(G) Par-3 edge polarity at boundary and non-boundary edges in control and *Ten-m* KD embryos.

A single average was calculated for each embryo and the mean ± SEM between embryos is shown. **p = 0.002, two-tailed Student's t test. n = 7 late stage 7 embryos per genotype in (D) (4–5 boundaries and 8–12 non-boundaries per embryo) and 7 early stage 7 embryos per genotype in (G) (33–67 boundary edges and 60–119 non-boundary edges per embryo). Embryos are early stage 7 in (A), (E), and (F) and late stage 7 in (C). Anterior left, dorsal up. Bars, 10 μm. See also Figures S4 and S5.

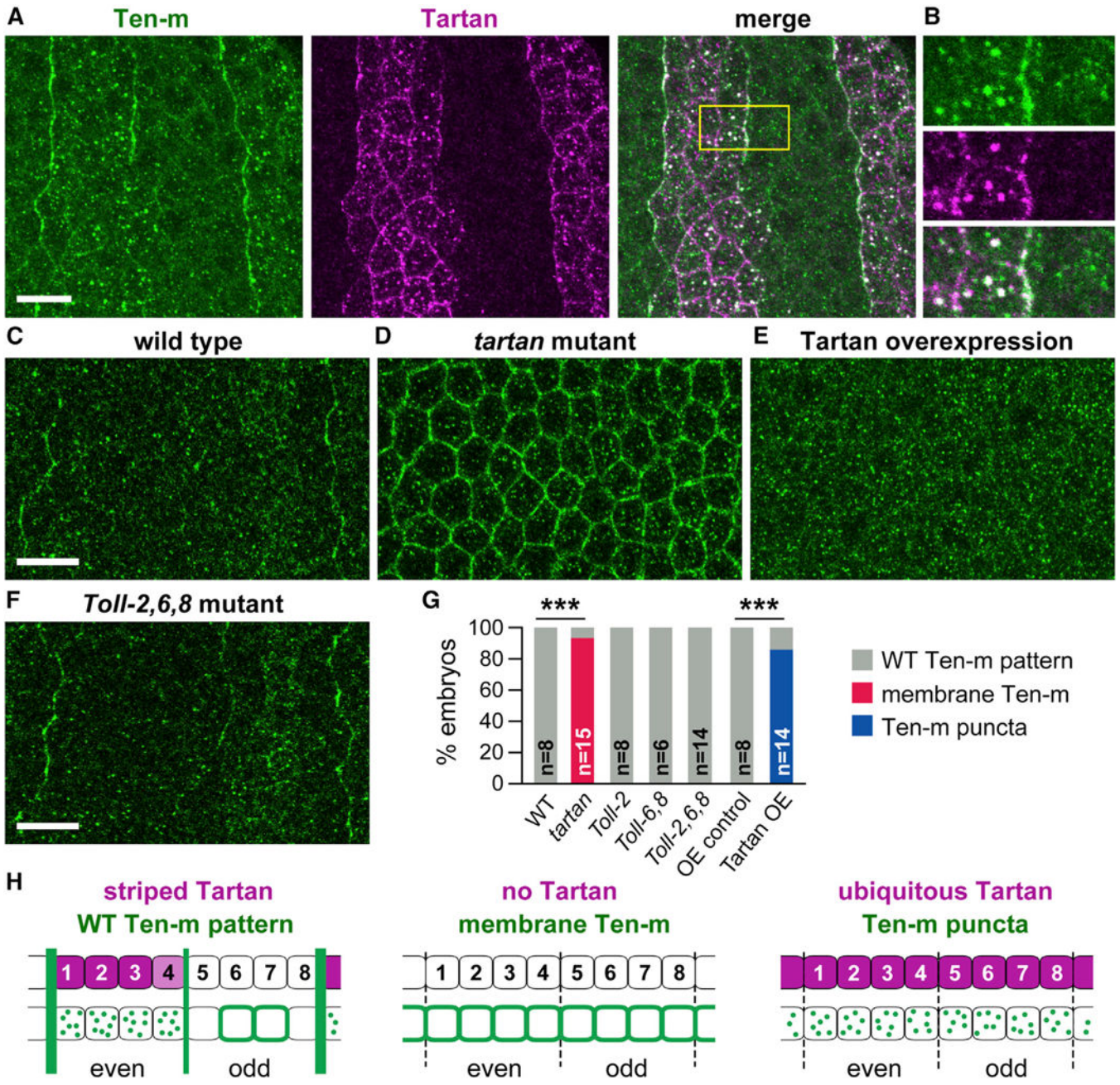

Figure 5. Ten-m Localization to Compartment Boundaries Requires Striped Tartan Expression

(A) Ten-m and Tartan protein localization (lateral plane).

(B) Close-up of a 15-μm-wide region flanking the 4/5 compartment boundary in (A).

(C–E) Ten-m localization in wild-type (C), *tartan* mutant (D), and Tartan-overexpressing (E) embryos. (F) Ten-m localization in a *Toll-2,6,8* mutant.

(G) Ten-m localization in the indicated genotypes (n = number of embryos analyzed). ***$p \leq 0.0001$ for *tartan* mutant embryos versus wild type (WT) and Tartan overexpressing (Tartan OE) embryos versus OE control, χ^2 test.

(H) Schematics of *tartan* expression and Ten-m localization. Genotypes: WT (Oregon R), *tartan* (*trn*^{3C}), *Toll-2* (*Toll-2*$^{\Delta 76}$), *Toll-6,8* (*Toll-8*^{59}, *Toll-6*^{1B}), *Toll-2,6,8* (*Toll-2*^{attP};

Toll-8$^{\Delta 6B}$, *Toll-6*^{attP}), OE control (maternal Gal4 alone), Tartan OE (embryos overexpressing Tartan–HA with a maternal Gal4 driver). All embryos are stages 7–8.
Anterior left, dorsal up. Bars, 10 μm. See also Figure S4.

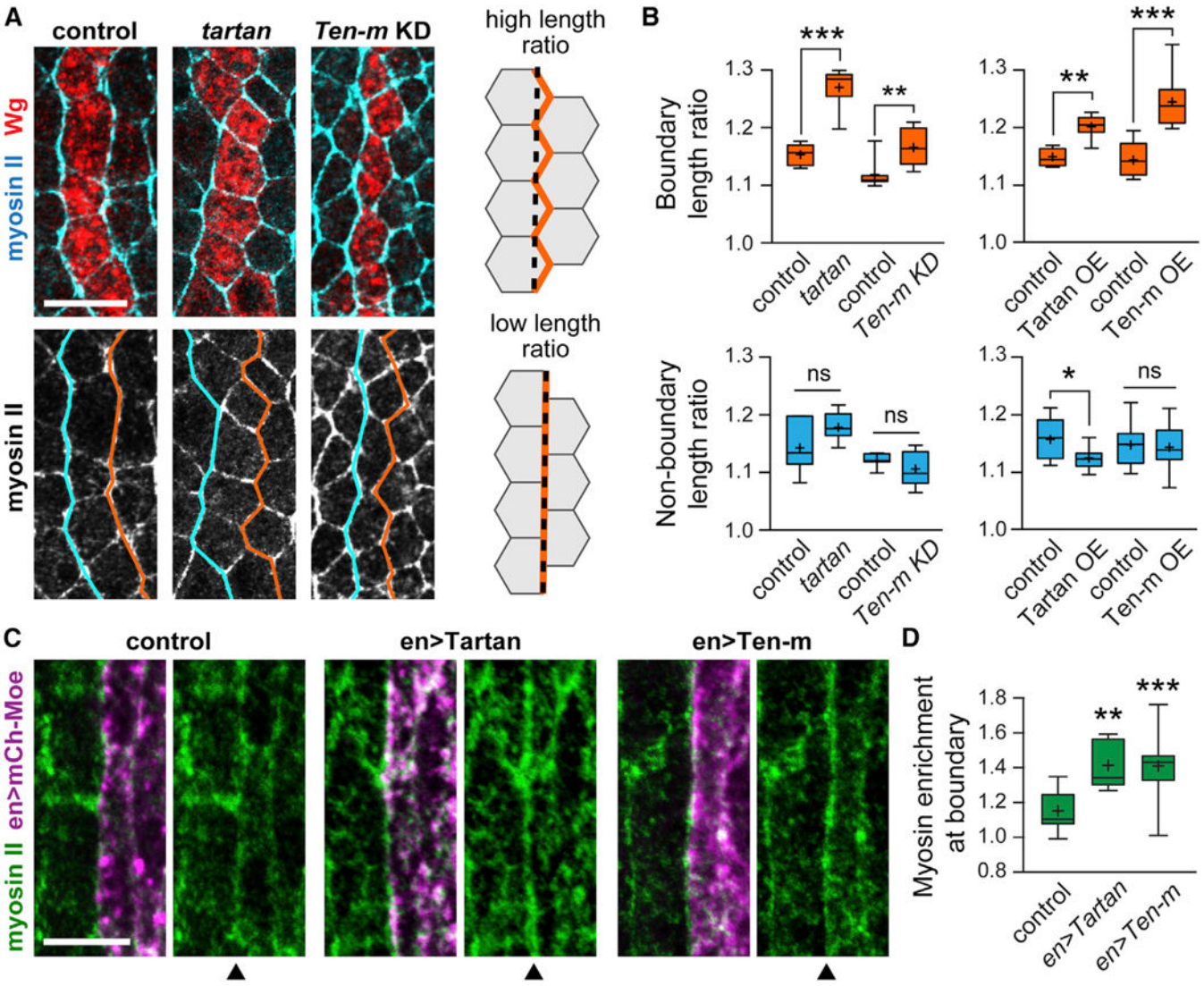

Figure 6. Tartan and Ten-m Regulate Myosin Localization and Cell Morphology at Compartment Boundaries

(A) Left, myosin II (myosin–GFP) and Wg protein in control, *tartan* mutant, and *Ten-m* KD embryos. Compartment boundaries, orange. Non-boundary interfaces, cyan. Right panels, length ratio is the measured length (orange) divided by shortest path (dashed line). Anterior left, dorsal up.

(B) The boundary length ratio (at the interfaces between columns 8 and 1 and between columns 4 and 5) and the non-boundary length ratio (at the interface between columns 7 and 8) are plotted for the indicated genotypes. Left plots, *tartan* mutant and *Ten-m* KD embryos. Right plots, Tartan-overexpressing (Tartan OE) and Ten-m-overexpressing (Ten-m OE) embryos. Appropriate controls were analyzed for each genotype (see STAR Methods).

(C) Myosin–GFP localization in stage 15 embryos expressing mCherry–Moesin alone (control) or mCherry–Moesin with Tartan–HA or HA–Ten-m under the control of the engrailed-Gal4 driver. Arrowheads, anterior boundary of the engrailed (en) domain. Anterior left, ventral views.

(D) Quantification of myosin–GFP enrichment at the anterior boundary of en stripes. A single mean value was obtained for each embryo and the distribution of mean values between embryos is shown in (B) and (D) (boxes, 25^{th}–75^{th} percentile; whiskers, 5^{th}–95^{th} percentile; horizontal line, median; +, mean). *p < 0.02, **p < 0.005, ***p < 0.0001, two-tailed Student's t test. n = 7–10 embryos per genotype in (B) (four boundaries and two 7/8 non-boundaries per embryo) and 7–15 embryos per genotype in (D) (2–5 engrailed stripes per embryo). Bars, 10 μm in (A), 5 μm in (C).

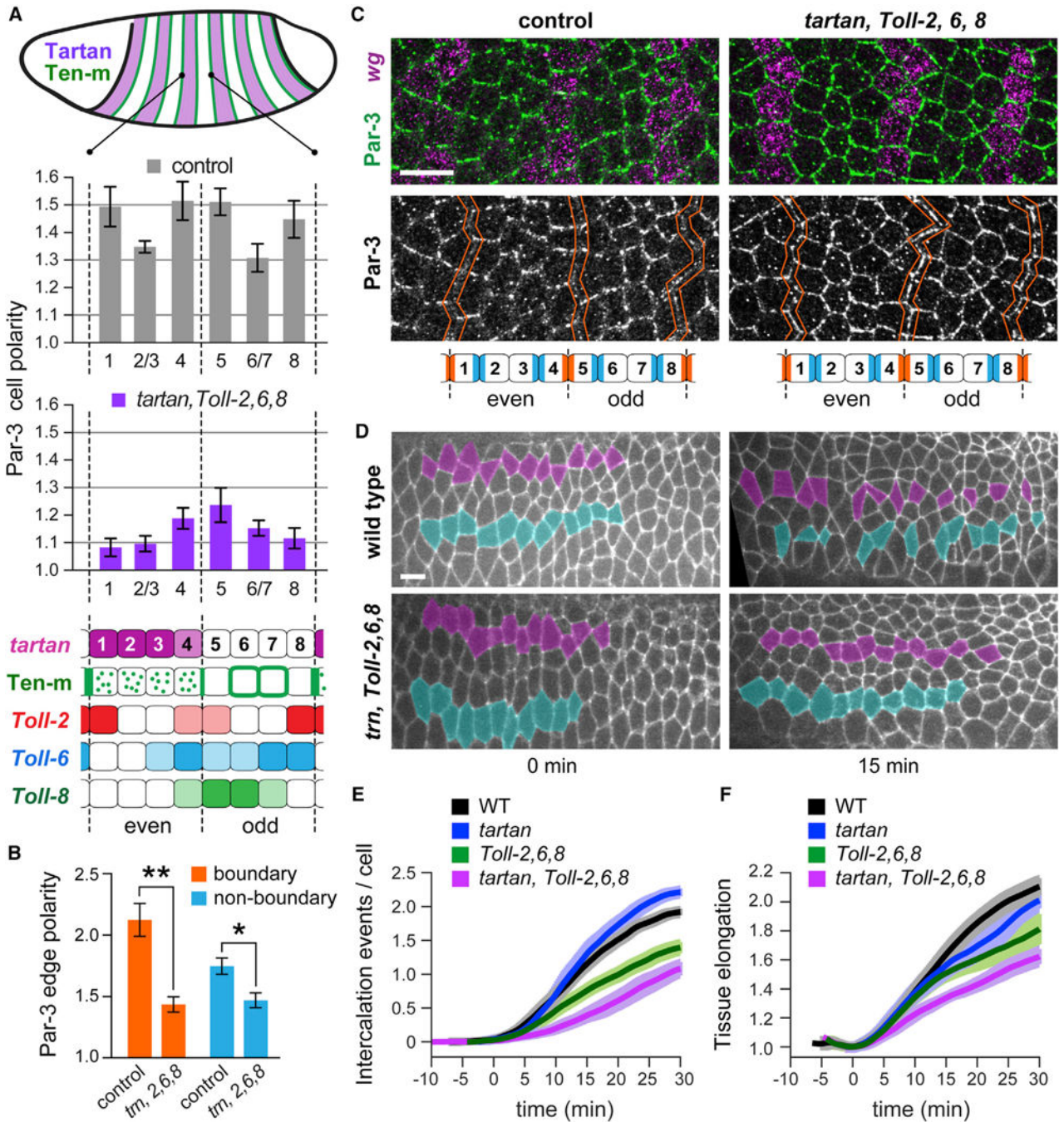

Figure 7. Tartan and Toll Receptors Independently Control Planar Polarity and Cell Intercalation

(A) Top, schematic of the relationship between Tartan and Ten-m at compartment boundaries. Bottom, *tartan* and Toll receptor expression and Ten-m localization in each double-compartment unit (bottom). Middle panels, Par-3 planar cell polarity was reduced in *tartan, Toll-2,6,8* quadruple mutants versus controls ($p < 0.005$ for all columns except 6/7, $p = 0.02$, two-tailed Student's t test).

(B) Par-3 edge polarity at boundary and non-boundary edges in control and quadruple-mutant embryos (*$p < 0.01$, **$p = 0.001$, two-tailed Student's t test).

(C) Par-3 protein and *wg* mRNA in control and quadruple-mutant embryos.
(D) Images from time-lapse movies of wild-type (WT) and quadruple-mutant embryos expressing Spider–GFP.
(E) Cumulative intercalation events per cell over time in WT, *tartan* single-mutant, *Toll-2,6,8* triple-mutant, and *tartan, Toll-2,6,8* quadruple-mutant embryos. $p < 0.02$ in *tartan* versus WT, $p < 0.0001$ in *Toll-2,6,8* versus WT, $p < 0.0001$ in *tartan, Toll-2,6,8* versus WT, $p < 0.01$ in *Toll-2,6,8* versus *tartan, Toll-2,6,8*.
(F) Tissue length normalized to the length at t = 0 in WT, *tartan* single-mutant, *Toll-2,6,8* triple-mutant, and *tartan, Toll-2,6,8* quadruple-mutant embryos. $p = 0.41$ in *tartan* versus WT, $p < 0.008$ in *Toll-2,6,8* versus WT, $p = 0.0003$ in *tartan, Toll-2,6,8* versus WT, $p = 0.11$ in *Toll-2,6,8* versus *tartan, Toll-2,6,8*. Uncorrected Fisher's LSD tests were performed using the final values at t = 30 min. t = 0 is the start of convergent extension in early stage 7. Mean ± SEM between embryos is shown, n = 7 early stage 7 embryos per genotype in (A) and (B) (10–62 cells in each category per embryo in A and 39–55 boundary edges and 77–115 non-boundary edges per embryo in B) and 3–7 embryos per genotype in (E) and (F) (194–406 cells tracked at least 12.5 min per embryo). Control in (A)–(C) (*Toll-2*^{attP}/+ or +/+; *trn*^{3A}, *Toll-8*$^{\Delta 6B}$, *Toll-6*^{attP}/+ or +/+); *tartan,Toll-2,6,8* in (A)–(C) (*Toll-2*^{attP}; *trn*^{3A}, *Toll-8*$^{\Delta 6B}$, *Toll-6*^{attP}), wild type in (D)–(F) (Spider–GFP and Spider– GFP/+), *tartan* in (E) and (F) (*trn*^{3C}, Spider–GFP), *Toll-2,6,8* in (E) and (F) (*Toll-2*^{attP}; *Toll-8*$^{\Delta 6B}$, *Toll-6*^{attP}, Spider–GFP), *tartan,Toll-2,6,8* in (D)–(F) (*Toll-2*^{attP}; *trn*^{3A}, *Toll-8*$^{\Delta 6B}$, *Toll-6*^{attP}, Spider-GFP). Embryos are early stage 7 in (C) and early stage 7 (0 min) or stage 8 (15 min) in (D). Anterior left, dorsal up. Bars, 10 μm. See also Figure S6.

KEY RESOURCES TABLE

REAGENT or RESOURCE	SOURCE	IDENTIFIER
Antibodies		
mouse monoclonal anti-digoxigenin	Jackson ImmunoResearch	200-002-156
mouse Living Colors mCherry antibody	Takara	632543
mouse monoclonal anti-Wingless	Developmental Studies Hybridoma Bank (Brook and Cohen, 1996)	4D4
mouse monoclonal anti-Ten-m	Levine et al., 1994	N/A
rabbit polyclonal anti-human placental alkaline phosphatase	ThermoFisher Scientific	PA1-29125
rabbit polyclonal anti-GFP	Torrey Pines	NC9589665
rabbit monoclonal anti-HA	Cell Signaling	C29F4
rabbit polyclonal anti-dinitrophenyl	ThermoFisher Scientific	A-6430
rabbit polyclonal anti-Tartan	Chang et al., 1993	N/A
guinea pig polyclonal anti-Par-3 (Baz)	Blankenship et al., 2006	N/A
guinea pig polyclonal anti-Tartan	Mao et al., 2008	N/A
rat monoclonal anti-HA	Sigma-Aldrich	3F10
Chicken polyclonal anti-GFP	Abcam	ab13970
AlexaFluor-488 Goat anti-mouse Secondary	Molecular Probes	A11001
AlexaFluor-488 Goat anti-rabbit Secondary	Molecular Probes	A11008
AlexaFluor-488 Goat anti-guinea pig Secondary	Molecular Probes	A11073
AlexaFluor-546 Goat anti-mouse Secondary	Molecular Probes	A11030
AlexaFluor-546 Goat anti-rabbit Secondary	Molecular Probes	A11035
AlexaFluor-647 Goat anti-guinea pig Secondary	Molecular Probes	A21450
Bacterial and Virus Strains		
Biological Samples		
Chemicals, Peptides, and Recombinant Proteins		
Critical Commercial Assays		
Deposited Data		
Experimental Models: Cell Lines		
D. melanogaster S2R+ cells	*Drosophila* Genomics Resource Center	Stock number 150
Experimental Models: Organisms/Strains		
D. melanogaster. Wild-type Oregon R strain	Bloomington *Drosophila* Stock Center	N/A
D. melanogaster. Toll-2^{attP}	This paper	N/A
D. melanogaster. Toll-6^{attP}	This paper	N/A
D. melanogaster. Toll-8^{59}	Yagi et al., 2010	N/A
D. melanogaster. Toll-8^{59} *, sqh-sqh-GFP*	This paper	N/A
D. melanogaster. Toll-8^{145}	Kolesnikov and Beckendorf, 2007	N/A
D. melanogaster. Toll-8$^{\Delta 6B}$, *Toll-6*^{attP}	This paper	N/A
D. melanogaster. Toll-8$^{\Delta 6B}$ *, Toll-6*^{attP} *, spider-GFP*	This paper	N/A

REAGENT or RESOURCE	SOURCE	IDENTIFIER
D. melanogaster. tartan ^{3C}	This paper	N/A
D. melanogaster. tartan^{3C}, *spider-GFP*	This paper	N/A
D. melanogaster. tartan^{3A}, *Toll-8*$^{\Delta 6B}$, *Toll-6*^{attP}	This paper	N/A
D. melanogaster. tartan^{3A}, *Toll-8*$^{\Delta 6B}$, *Toll-6*^{attP}, *spider-GFP*	This paper	N/A
D. melanogaster. UASp-tartan-HA (VK37) (II)	This paper	N/A
D. melanogaster. UASp-HA-Ten-m (attP2) (III)	This paper	N/A
D. melanogaster. Ten-m-GFP $^{CPTI-001175}$	Lye et al., 2014	N/A
D. melanogaster. sqh-sqh-GFP (II)	Royou et al., 2004	N/A
D. melanogaster. engrailed-Gal4, UASp-mCherry-Moesin (II)	Millard and Martin, 2008	N/A
D. melanogaster. eve-YFP BAC (attP2) (III)	Ludwig et al., 2011	N/A
D. melanogaster. spider-GFP (III)	gift of Alain Debec	N/A
Oligonucleotides		
See Table S1		
Recombinant DNA		
Plasmid. *pECIA14*	Ozkan et al., 2013	N/A
Plasmid. *pUASp-tartan-HA*	This paper	N/A
Plasmid. *pUASp-HA-Ten-m*	This paper	N/A
Plasmid. *pMT-Tartan-AP5*	This paper	N/A
Plasmid. *pMT-AP5-Ten-m*	This paper	N/A
Plasmid. *pENTR-Toll-2*	Paré et al. 2014	N/A
Plasmid. *pENTR-Toll-6*	Paré et al. 2014	N/A
Plasmid. *pENTR-Toll-8*	Paré et al. 2014	N/A
Plasmid. GH10871 (*pOT2-tartan*)	BDGP Gold Collection	*Drosophila* Genomics Resource Center
Software and Algorithms		
SEGGA	Farrell et al., 2017	N/A
SIESTA	Fernandez-Gonzalez and Zallen, 2011	N/A
ImageJ and Fiji	Schneider et al., 2012	https://imagej.nih.gov/ij/
Prism 7	Graphpad	N/A
Matlab	Mathworks	N/A